# A thermal diode based on phase change materials: from 2D simulations to 3D prototyping

Luís Afonseca
Mestrado em Engenharia Física
Departamento de Física e Astronomia
2023

**Orientador**
João Oliveira Ventura, Investigador Principal
Faculdade de Ciências da Universidade do Porto

**Coorientador**
Daniel José da Silva
Faculdade de Ciências da Universidade do Porto

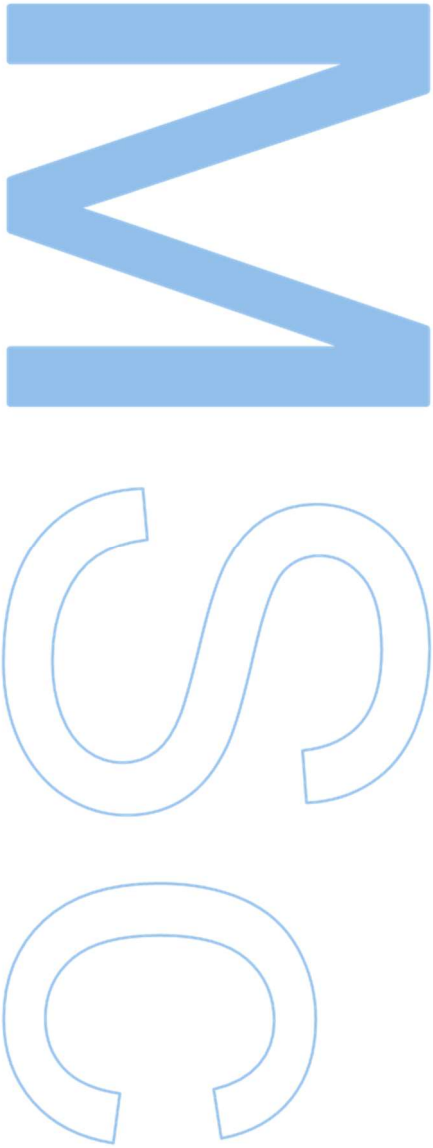

*" When Life Gives You Lemonade, Make Lemons. Life Will Be All, 'Whaaat?' "*

Phil Dunphy,
Modern Family

# *Acknowledgements*

First and foremost, I want to express my deepest gratitude to my supervisor, Professor Dr. João Ventura, for his insights, fruitful discussions, mentoring, and the occasional words of encouragement and motivation during the most stressful times. It has been a huge pleasure working with you over the past year and a half. This gratitude is also extended to my co-supervisor Dr. Daniel Silva, with whom I have been working since my fourth year, for his tremendous contribution to my academic and personal development, and for making me a better programmer.

It is unavoidable to thank all the researchers and staff associated with IFIMUP that helped me throughout the past few months. I would like to thank Cláudia Fernandes for all the help with the numeric simulations, Fernando from the department's workshops for turning my prototype design into reality, and all the people from Lab. 118, especially Afonso, Andreia and Maria, for the countless hours we spent together either working on our experiments or chatting outside the department during those hot summer afternoons.

On a personal note, I want to thank all my friends that filled these past five years with the most joyful and rewarding memories. Firstly, I want thank my cousins, André and Miguel, for all the time we spent together during the dark times of the 2020 lock-down and for always finding a way of making me laugh. To all the lovely people from "Mansão", thank you for all the unforgettable moments we have shared and for helping me go through the hardest moments of my academic life. Diogo, Júlio and Raúl, I am grateful for the many memories I will take from the hardworking hours at the 'salinha', and for all the coffee breaks, movie nights, dinners and parties.

It is now the time to express my deepest gratitude to the three people without whom I would certainly not have come this far. Firstly, I want to thank Deus for all those times we both fell asleep on the subway, for the late nights we spent trying to solve the same Quantum Mechanics exam for the third time, and for being one of the most transparent and inspiring people I've ever met. Nico, thank you for all the chats we had about music, movies, Legos, nerdy tech stuff, for having the most contagious laugh I have ever heard, and for all the times I bothered you with dumb physics questions. And Tixa, although a small paragraph is a bit of an insult to what you truly deserve, I want to thank you not only for the countless reports, projects, and presentations we did together, where you pushed me to be a better version of myself but also for being the best friend I ever had

and for always being there, whether I needed it or not. Thank you for the texts, calls, the many hours we spent watching Modern Family and Formula 1, and for the many moments I lived by your side.

Finally, to my family, I thank you for the unconditional support you have given me since this whole journey started. Mãe, Pai, Inês and Sirius, I want you to know that despite my usual grumpiness in these recent times, I will always be grateful for the effort you have put into my happiness and well being.

UNIVERSIDADE DO PORTO

# *Abstract*

Faculdade de Ciências da Universidade do Porto
Departamento de Física e Astronomia

MSc. Engineering Physics

**A thermal diode based on phase change materials: from 2D simulations to 3D prototyping**

by Luís AFONSECA

In several technological and industrial areas that employ thermal management systems, the demand for efficient temperature control has never been more critical. To address this need, the emergence of Phase Change Materials (PCMs) as the basis for thermal diodes (TDs) has garnered significant attention. These devices utilize the ability of PCMs to absorb or release latent heat during phase transitions, to create a dynamic and responsive solution for thermal regulation. This way, thermal diodes based on PCMs offer a promising avenue for monitoring operating temperatures and enhancing energy efficiency.

Thus, our work focuses on designing, simulating, and building a PCM-based structure that showcases the characteristic rectifying behavior of a TD. Our concept consists in a squared sink, made of a thermal conductive material, with equally spread PCM reservoirs that are surrounded by a thermal insulating material. This arrangement of materials provides a spacial asymmetry in thermal conductivity, which is a condition for thermal rectification. As part of this research, we used the *heatrapy* Python framework to compute the heat transfer phenomena of a simple two-dimensional structure composed of aluminum, vacuum and water, as thermal conductor, thermal insulator and PCM, respectively. The initial design, tested for single value of temperature bias ($\Delta T = 10$ K), showed a considerable difference in thermal energy density between the *forward* and *reverse* modes. Moreover, representing the thermal rectification ratio as a function of the triggering temperature, it was found that higher temperature variations lead to a decrease in performance, with 60% being the maximum value. We computed the transfer function

of the device and it demonstrated the TD characteristic nonlinear profile of the heat flow rate. Furthermore, we studied the impact of a handful of geometrical parameters and properties in the device's performance. Here, we tested alternative materials for the thermal insulation role, which showed not to have any influence in the performance. As to the fraction of PCM, it led to an increase of both the rectification ratio (12-170%) and the time needed for phase transition to occur (0-8 h). The same result was obtained for the fraction of insulating material, however its impact on the rectification ratio was not so severe (40-42.5 %). Reaching a final optimized design and verifying its nonlinear transfer function, a series of COMSOL simulations were done to determine the minimum thickness that a three-dimensional version of the device needed to have. Making some adjustments to the design to account for technical issues, the device was built and the assembled data acquisition setup allowed to measure the temperature variations and compute thermal and power densities for the two directions of heat flow. It was found that the ice-water phase transition paired with the asymmetric design of the thermal insulator shells, led to notable differences in thermal power and thermal energy densities between the two configurations (200 kW/m), demonstrating the intended nonlinear thermal properties of the device.

This way, our work was able to demonstrate a viable geometry that could be implemented in a TD-based thermal management system. Additionally, we showed that the particular set of materials that were used and the way they were assembled fulfills the criteria for thermal rectification and leads to a good performance.

UNIVERSIDADE DO PORTO

# *Resumo*

Faculdade de Ciências da Universidade do Porto
Departamento de Física e Astronomia

Mestrado Integrado em Engenharia Física

**Um díodo térmico baseado em materiais de transição de fase: de simulações 2D a prototipagem 3D**

por Luís AFONSECA

Em várias áreas tecnológicas e industriais que utilizam sistemas de gestão térmica, a procura por um controlo eficiente da temperatura nunca foi tão crítica. Para abordar esta necessidade, o surgimento de Materiais de Transição de Fase (MTFs) como base para diodos térmicos (DTs) tem recebido uma atenção significativa. Estes dispositivos utilizam a capacidade dos MTFs para absorver ou libertar calor latente durante transições de fase, criando assim uma solução dinâmica e responsiva para a regulação térmica. Desta forma, os diodos térmicos baseados em MTFs oferecem uma via promissora para monitorizar temperaturas de funcionamento e melhorar a eficiência energética.

Assim, o nosso trabalho concentra-se no design, simulação e construção de uma estrutura baseada em MTFs que demonstre o comportamento retificador característico de um DT. O nosso conceito consiste numa calha quadrada, feita de um material condutor térmico, com reservatórios de MTFs igualmente distribuídos, rodeados por um material isolante térmico. Esta disposição de materiais proporciona uma assimetria espacial na condutividade térmica, que é uma condição para a retificação térmica. Como parte desta pesquisa, utilizamos o framework Python Heatrapy para calcular os fenómenos de transferência de calor de uma estrutura bidimensional simples composta por alumínio, vácuo e água como condutor térmico, isolador térmico e MTF, respetivamente. O design inicial, testado para um único valor de desvio de temperatura ($\Delta T$ = 10 K), mostrou uma diferença considerável na densidade de energia térmica entre os modos direto e inverso. Além disso, ao representar a razão de retificação térmica como uma função da temperatura de acionamento, constatou-se que maiores variações de temperatura levam a uma diminuição de desempenho, com 60% sendo o valor máximo. Calculamos a

função de transferência do dispositivo e esta demonstrou o perfil não linear característico de um DT na taxa de fluxo de calor. Além disso, estudamos o impacto de um punhado de parâmetros geométricos e propriedades no desempenho do dispositivo. Aqui, testamos materiais alternativos para o papel de isolamento térmico, que não demonstraram ter qualquer influência no desempenho. Quanto à fração de MMFs, esta levou a um aumento tanto da razão de retificação (12-170%) como do tempo necessário para ocorrer a transição de fase (0-8 horas). O mesmo resultado foi obtido para a fração de material isolante, no entanto, o seu impacto na razão de retificação não foi tão severo (40-42,5%). Alcançando um design final otimizado e verificando a sua função de transferência não linear, foram realizadas uma série de simulações COMSOL para determinar a espessura mínima que uma versão tridimensional do dispositivo precisava ter. Fazendo alguns ajustes ao design para resolver problemas técnicos, o dispositivo foi construído e o setup de aquisição de dados montado permitiu medir as variações de temperatura e calcular as densidades térmicas e de potência para as duas direções do fluxo de calor. Verificou-se que a transição de fase gelo-água emparelhada com o design assimétrico das carapaças isolantes térmicas levou a diferenças notáveis na densidade de energia térmica entre as duas configurações, demonstrando as propriedades térmicas não lineares pretendidas do dispositivo.

Desta forma, o nosso trabalho conseguiu demonstrar uma geometria viável que poderia ser implementada num sistema de gestão térmica baseado em DTs. Além disso, mostrámos que o conjunto particular de materiais que foi utilizado e a forma como foram montados cumpre os critérios para a retificação térmica e conduz a um bom desempenho.

# Contents

# List of Figures

# List of Tables

# Glossary

| | |
|---|---|
| **TD** | Thermal Diode |
| **TR** | Thermal Regulator |
| **TS** | Thermal Switch |
| **PCM** | Phase Change Material |
| **FGM** | Functionally graded materials |
| **SC** | Superconductor |
| **PV** | Photovoltaic |
| **MCM** | Magnetocaloric Material |
| **TES** | Thermal Energy Storage |
| **SHTES** | Sensible Heat Thermal Energy Storage |
| **LHTES** | Latent Heat Thermal Energy Storage |
| **LHS** | Latent Heat Storage |

# Chapter 1

# Introduction

## 1.1 Motivation

One of the foremost obstacles in contemporary technology has been enhancing the performance of thermal management systems. From energy generation and storage systems to manufacturing machinery and data storage devices, many are the domains where performance and efficiency are extremely dependent on well-optimized heat dissipation mechanisms [1–3]. However, engineers seeking better solutions to direct heat flow are limited by the traditional toolkit of thermal appliances that rely on heat sinks and fluids for that purpose, e.g., water or fan coolers, which belong to the group of linear, stationary, and passive thermal components[4, 5]. These devices present many drawbacks, namely the hydraulic components, mechanical moving parts, and structural limitations of the used materials, which end up compromising the efficiency of thermal energy management [6, 7].

The vast array of highly nonlinear, switchable, and active thermal components that are accessible in the electrical domain encouraged researchers to start thinking about other possibilities on which to base thermal management systems. For example, integrated circuits rely on transistors, switches, and diodes for information processing and power transmission. However, thermal components of the same kind are not nearly as evolved as their electrical counterparts.

Over the past two decades, there has been a considerable increase in research with the aim of integrating switchable and nonlinear components in the thermal management domain. In this category, the thermal diode has drawn massive interest over the years (Fig. 1.1). Analogous to the electrical diode, this device exhibits thermal rectification, which can be defined as heat transport characterized by a preferential direction for heat

flow [8, 9]. This way, it is not only able to dissipate the excess heat from the system but also to block heat from flowing to the system. To achieve thermal rectification, one must fulfill two main criteria: spatial asymmetry and nonlinear thermal conductivity [10]. Considering these factors, phase-change materials (PCMs), which can exist in two states with different thermal conductivities, are pointed out as a unique opportunity to realize nonlinear thermal transport. It was already shown by Dames [11] that the performance of a thermal diode made of two different materials is influenced by three main factors: the difference between the temperature-dependent thermal conductivities, the difference in thermal resistance, and the temperature gradient. As a result, the combination of a PCM and a non-PCM or two PCMs can result in thermal rectification [8].

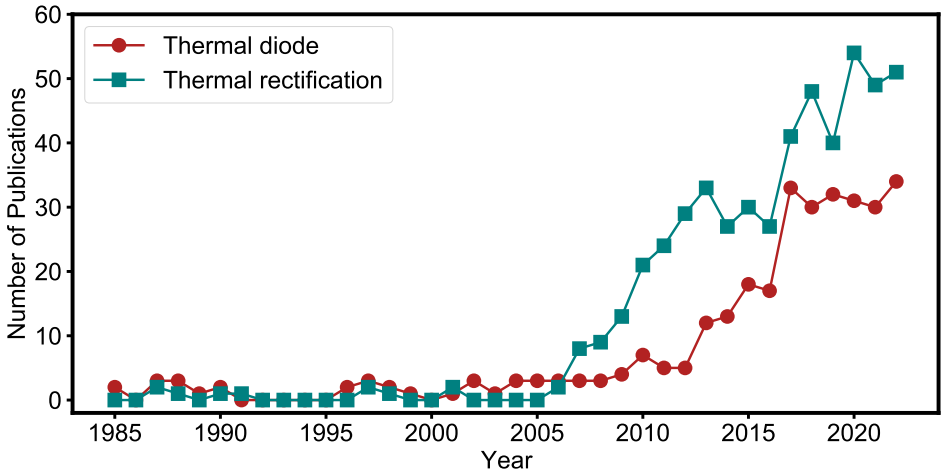


FIGURE 1.1: Number of publications on thermal diodes and thermal rectification per year since 1975. Data available in *Scopus*.

## 1.2 Objective

With the promising qualities that PCM-based thermal diodes have shown [12–14], we will be pursuing a deep computational and experimental study of system that consists in an aluminum (thermal conductor) heat sink that includes water (PCM) reservoirs surrounded by acrylic (thermal insulator) shells. The arrangement of this materials is designed to achieve a nonlinear spacial thermal conductivity, which is a condition for thermal rectification. The study of its performance will be done trough the evaluation of several parameters, such as the device's geometry, the insulating materials, PCM amount,

ambient temperature, and bias temperature. With the aim of demonstrating that this combination of materials is a viable choice for a thermal diode setup several simulation scripts were developed, a device was engineered, and a measuring setup was constructed.

## 1.3 Document overview

The **first** and introductory chapter includes a brief explanation of the motivation behind all the work presented in the dissertation and its main goals. Following this, the **literature review chapter** gives an overview of the published material related to the subject in study, mainly associated with the so-called nonlinear and switchable thermal components, and discusses the thermal diode in more detail. This chapter also presents the main advantages of phase-change materials in thermal management applications.

The **third** and **fourth** chapters are related to the computational part of this work. The third chapter presents and explains the main idea of this dissertation, and the concept validation results are discussed. The fourth chapter has to do with all the parameters that were varied in the numerical simulations, from materials to geometrical aspects of the device, and includes the results and analysis of those simulations.

The **fifth** chapter relates to the experimental part of the work, dealing with the explanation of the building process of the prototype, the executed measurements, the measuring setup that was used, and the data analysis pipeline. The main results obtained from the experimental work are also discussed in this chapter.

Lastly, the chapter on **conclusions and future work** is intended to give an outline of the main conclusions drawn from the results of both computational and experimental work. It also mentions the future work necessary not only to fill the gaps in knowledge that came up in this experiment but also to enrich the quality and novelty of this work.

# Chapter 2

# Recent Trends in Heat Control

## 2.1 Nonlinear and switchable thermal components

As briefly mentioned in the previous chapter, both switchable and nonlinear thermal components are responsible for great research enthusiasm in the field of thermal management systems due to their unique properties. Figure 2.1 displays the commonly used symbols, transfer functions, and illustrations of heat conduction mechanisms for the thermal diode, regulator, and switch. In the following sections, it is given a brief description of the working principles of each of these devices, as well as the respective figures of merit, commonly used materials, and applications. The thermal diode, being the focus of this thesis, will be discussed in greater detail.

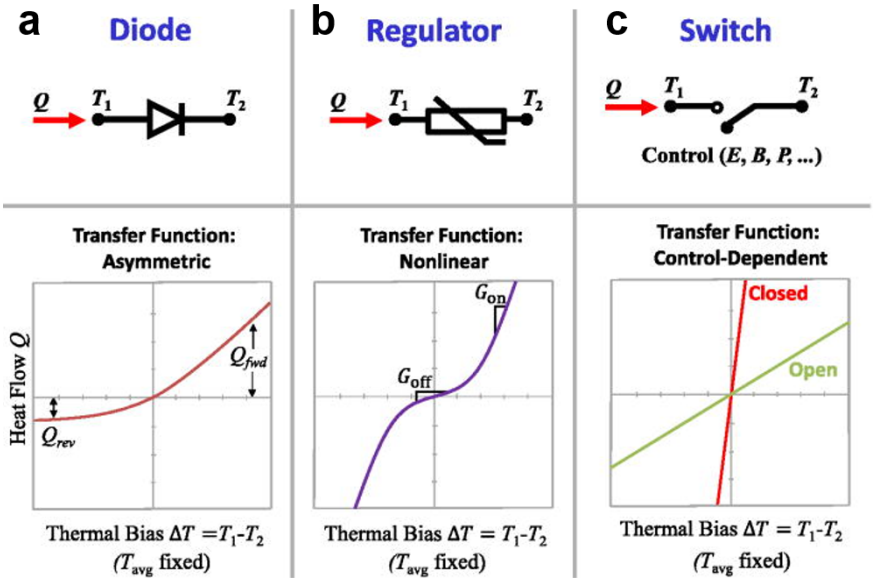


FIGURE 2.1: Nonlinear and switchable thermal components: **(a)** thermal diode, **(b)** thermal regulator and **(c)** thermal switch. Adapted from [15].

### 2.1.1 Thermal Regulator

As illustrated Fig. 2.1(b), a thermal regulator is essentially a two-terminal device that is capable of maintaining an intended critical temperature $T_C$ by switching between high and low conductance states. These devices have a highly nonlinear transfer function * at a fixed average temperature $T_{avg} = (T_h + T_c)/2$, where $T_h$ is the temperature of the hot side and $T_c$ is the temperature of the cold side. A typical figure of merit for a TR is the on/off switching ratio:

$$r = \frac{G_{\mathbf{on}}}{G_{\mathbf{off}}} \tag{2.1}$$

where $G = dQ/d(\Delta T)$ represents the differential thermal conductance ($G$), which is defined as the local slope of the transfer function (Fig. 2.1(b)). In terms of thermal conductance, this figure of merit represents the ratio of the *on* state to the *off* state [15], and can also be defined as the ratio of the differential thermal resistance between the *off* and *on* states, respectively [16]. Phase change materials (PCMs) with sharp changes in thermal conductivity ($k$), at a critical temperature $T_c$ (Fig. 2.2(a)) are often excellent candidates for thermal regulation. In these cases, the application aspect of the TR implies a minimization of the phase transition hysteresis, in a way that the temperature is regulated at the same $T_c$.

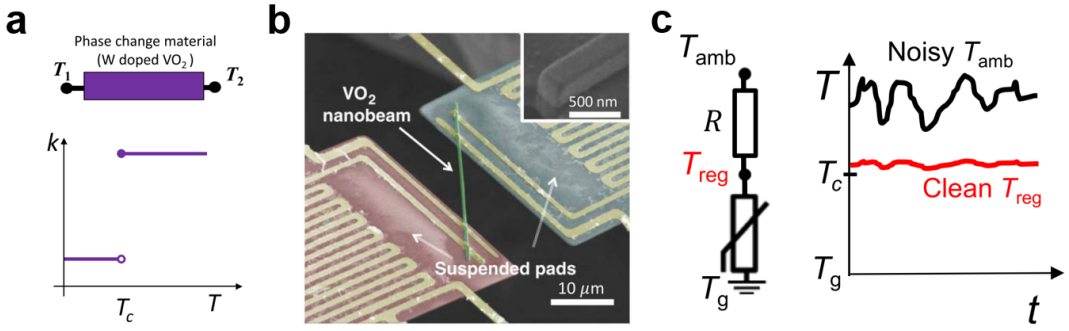


FIGURE 2.2: **(a)** schematic representation of a W-doped $VO_2$ thermal regulator and the sharp $k$ change of the used PCM. **(b)** Scanning electron microscope (SEM) image of the of the doped TR [17]. **(c)** Thermal circuit where a TR is used to maintain a regulated temperature $T_{reg}$ in the presence of a noisy ambient temperature $T_amb$ [18].

Electric regulators are often employed to provide stable voltage sources, much as it is for the electrical components. Similar to this, TRs can be used to reduce temperature variations in situations like manufacturing applications, climate control, and precision tests where a constant temperature is required [15]. An example of a thermal circuit where

*Relates the heat flow ($Q$) and the triggering temperature difference ($\Delta T$) across the device

a TR is used to damp out unwanted ambient temperature fluctuations is illustrated in Fig. 2.2(c).

### 2.1.2 Thermal Switch

A thermal switch (Fig. 2.1(c)) can be briefly described as a component that can switch between low and high thermal conductivity, corresponding to *off* and *on* states, respectively. These devices depend on a non-thermal external trigger, such as a magnetic field, electric field, applied pressure or light [19]. By adjusting the control parameter, one can change the thermal conductance of the device and either reduce (low $k$) or facilitate (high $k$) the heat flow. In Fig. 2.3 one can identify the drastic change in $k$ that two different TSs showcase when triggered by light and magnetic field. The materials available to build these devices are selective to the control parameter, which go from ferroelectric and ferromagnetic materials to PCMs and polymers [19].

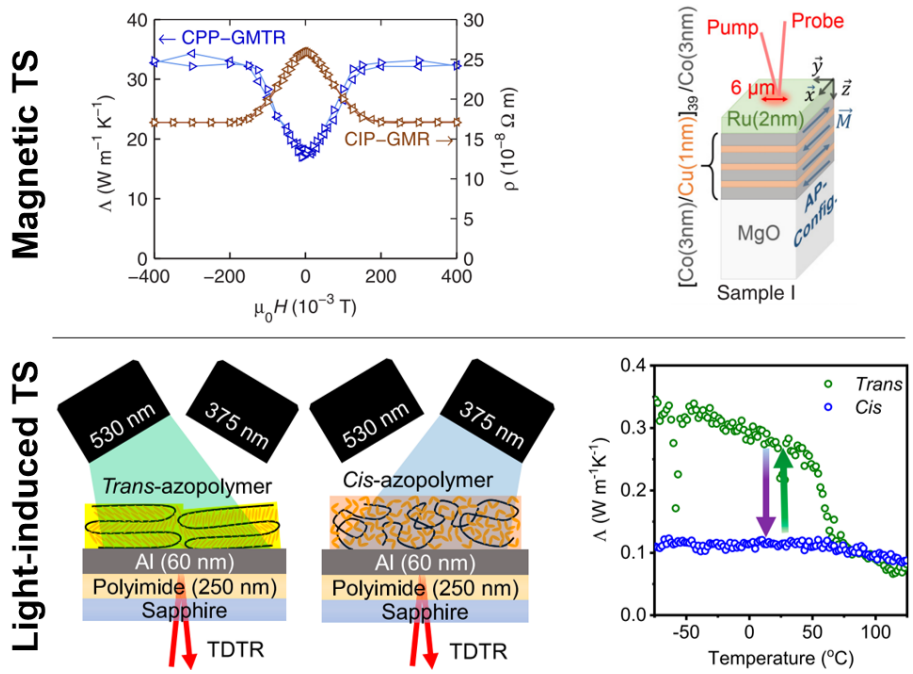


FIGURE 2.3: Examples of TSs with different triggering parameters. **Top**: Cross section and $k$ variation of a giant magnetoresistance (GMR) device where the magnetic field direction controls the thermal transport [20]. **Bottom**: TS through light sensitive polymer structures, which affect $k$ according to the color of the light [21].

Switching between two states of different thermal conductivities is a feature useful in a variety of scenarios ranging from spacecraft applications [22] to heat engines [15] and cryogenics [23]. Among the many advantages of these devices, it is worth mentioning the versatility of switching trigger parameters and the absence of moving parts. As to

the disadvantages, the switching ratio, which is the same figure of merit introduced in the previous section of the TR, is still quite low at room temperature, which limits their application range [19].

### 2.1.3 Thermal Diode

As it was briefly mentioned in chapter 1, a thermal diode/rectifier (Fig. 2.1(a)) can be shortly described as a device able to rectify heat flux, i.e., a device that exhibits the phenomenon of thermal rectification. Thermal rectification refers to nonlinear heat transfer along an axial direction of the device, meaning that heat flows more easily in one direction than the other. The thermal transport along this specific axis depends on the sign of the temperature gradient or heat current, i.e., forward ($Q_{fwd} : T_1 > T_2$) versus reverse ($Q_{rev} : T_2 > T_1$) direction [8, 15, 19]. The thermal rectification ratio is the commonly used figure of merit that quantifies the performance of TDs, here defined as:

$$\gamma = \frac{|Q_{fwd}| - |Q_{rev}|}{|Q_{rev}|}, \tag{2.2}$$

where $Q_{fwd}$ is greater than $Q_{rev}$ for the same thermal bias $|\Delta T|$, which is the temperature difference across the device [15].

Due to the asymmetric heat flux already mentioned, TDs are able to function as a thermal insulator, preventing heat from entering the system, while also facilitating the dissipation of excess heat. As a result, these devices can maintain the temperature of the system at the desired level. The operation of TDs is illustrated Fig. 2.4, along with a comparison to the equivalent device of the electronic domain. The following sections will go into greater details on the requirements for developing a thermal diode, as well as the working principles of the different types of TDs and their applications.

#### 2.1.3.1 Designing a thermal rectifier

As mentioned, a thermal diode or thermal rectifier is a device that allows heat to flow in one direction more easily than in the other. At a glance, the idea that it is possible to build a solid-state device with such capabilities may sound counter-intuitive. Peyrard, however, not only demonstrated that the construction of a thermal rectifier can be theoretically understood through fundamental laws of heat conduction, but also outlined a number of requirements that must be used to design a TD [10].

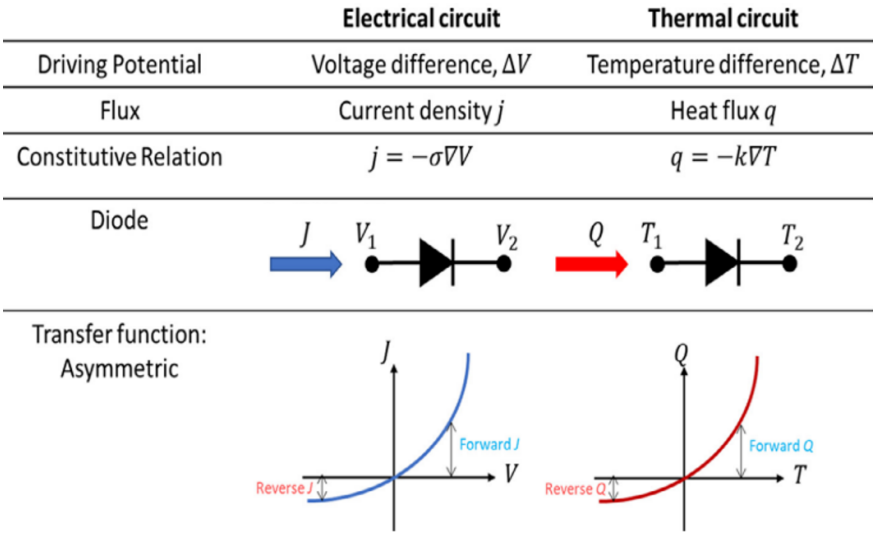


FIGURE 2.4: Comparison between electrical and thermal diodes. Adapted from [8].

Essentially, there are two main requirements that must be met for thermal rectification to occur. Firstly, the device needs to have an **asymmetric structure** along the heat flow direction. A common example is the so-called two-segment TD, which consists in a joint of two dissimilar materials (Fig. 2.5(b)). Secondly, the heat transfer performance of the device must be spacial- and temperature-dependent. An intuitive way of fulfilling this last criterion is to use materials with a **temperature-dependent thermal conductivity**, such as composite materials or solids in the vicinity of a phase transition. Apart from using different materials in the same device to achieve spatial asymmetry, exploring the geometry of the device can also have practical advantages. For instance, it is possible to build a TD made of a conducting material with different layer widths and shapes, which introduce an additional spacial dependency in $k$ (Fig. 2.5(a)).

These criteria suggest that a functional thermal diode can be built through the selection of the best materials and device shapes. However, it should be noted that there is no assurance of thermal rectification even if the device complies with the requirements listed in the previous paragraph.

#### 2.1.3.2 Types of thermal diodes

Thermal diodes can be divided, according to the predominant heat transfer mechanism, into three main groups: **conduction**, **convection**, and **radiation**. In this section each of

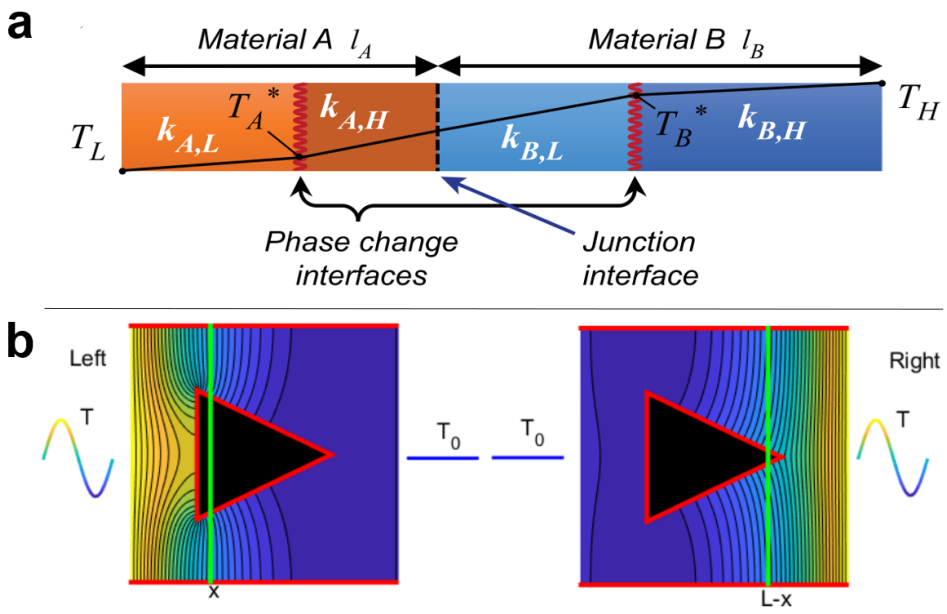


FIGURE 2.5: **(a)** Heatmaps for *forward* (left) and *reverse* (rigth) modes of an asymmetrically shaped TD [24]. **(b)** Schematic representation of a two-sided TD [25].

these types of TDs is covered, as well as the respective working principles, used materials and structures (Fig. 2.6). In each case, the literature and performance measuring parameters are presented.

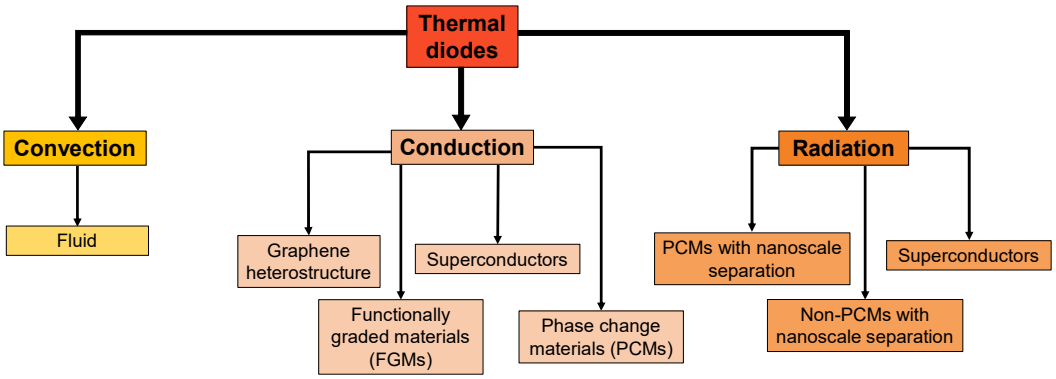


FIGURE 2.6: Schematic diagram of the types of thermal diodes and some materials that are used for each category.

Firstly, **conduction TDs** are thermal diodes that have thermal conduction as the main heat transfer mechanism, where thermal conduction is the heat transport process that happens through molecular vibration and movement of free electrons in a metal [26]. The main characteristics of these diodes that contribute to thermal rectification are, as it was previously mentioned, the asymmetric thermal conductivity and phonon propagation, which are severely dependent on the properties of the used materials and the structure of the device. As indicated in Fig. 2.6, conductive TDs can be built using different structures

and materials which lead to different rectification behaviors and performances (Table 2.1). Graphene is a very popular material in the field of thermal management systems due to its extremely high thermal conductivity (3000-5000 W/m·k), an order of magnitude higher than that of copper, making it a good candidate for TD devices [27]. A **graphene heterostructure** TD was fabricated focusing on the asymmetric interfacial heat transfer characteristics between two similar/dissimilar materials, where thermal rectification arises trough asymmetric phonon propagation in different direction across the interface (Fig. 2.7(a)). Rows 1 to 3 in table 2.1 indicate the figure of merit for studies done with these structures, where the responsible mechanism and the used materials are also indicated.

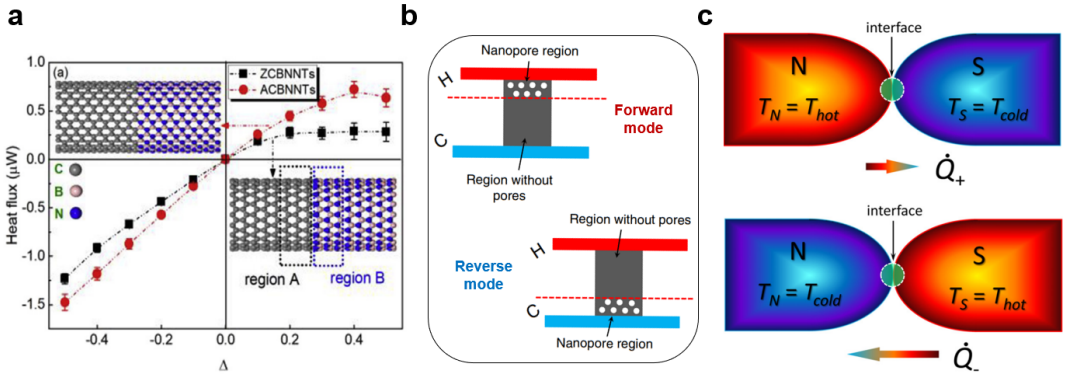


FIGURE 2.7: **(a)** Transfer functions of heterostructures made of carbon nanotubes [28]. **(b)** Illustration of an FGM-based TD in forward and reverse directions [29].**(c)** Forward and reverse directions of a metal-superconductor nanojunction [30].

| Type of TD | Used materials | $\gamma^a$ | References |
|---|---|---|---|
| Conduction | Graphene heterostructure | 0.3 | [31] |
| | FGMs | 0.65 | [32] |
| | Superconductors | 1.23 | [30] |
| Convection | Fluid | 38 | [33] |
| | | 1.42 | [34] |
| | | 250 | [35] |
| Radiation | PCMs | 1 | [36] |
| | Non-PCMs | 1.5 | [37] |
| | Superconductors | 4 | [38] |

[a] Calculated according to eq. 2.2.

TABLE 2.1: Summary of a few examples of thermal rectification ratios of TDs, of different types and made of various materials.

Still in the conductive TDs category, one shall briefly discuss the interest in using functionally graded materials (FGMs) as well as superconductors. FGMs are materials with a composition gradient (porosity, doping, geometry, etc) along a certain axis and have, among other properties, spatially-dependent thermal conductivity, fulfilling the criteria for thermal rectification (Fig. 2.7(b)). As to superconductors, their novel properties and

the fact that their thermal and optical responses change after phase transitions, make them suitable materials for TDs where they can be paired with other materials (Fig. 2.7(c)). In table 2.1 we have also included relevant literature studies on TDs using these materials. Since PCM-based TDs are the main focus of this thesis, their properties and mechanisms will be later introduced in section 2.2.

Now, we introduce **convective TDs**. These diodes are devices that have thermal convection as the main heat transfer process [39], where thermal convection can be defined as a mechanism of heat transfer through a fluid in the presence of bulk fluid motion. The presence and behavior of a fluid contributes to an asymmetrical heat transport mechanism, meaning that thermal rectification can be observed (Fig. 2.8). A simple example of a fluid-based convective thermal diode is a chamber filled with some kind of thermal fluid, such as water, oil or nanofluids [8]. These devices, as it is discussed in the next section, are often employed in solar heating systems due to their heat transfer performances, particularly in the forward direction. Table 2.1 includes a few examples of fluid-based convection TDs that can be found in literature, and one can verify by the rectification ratios that, depending on the fluid, device structure and the materials used, the performance varies dramatically.

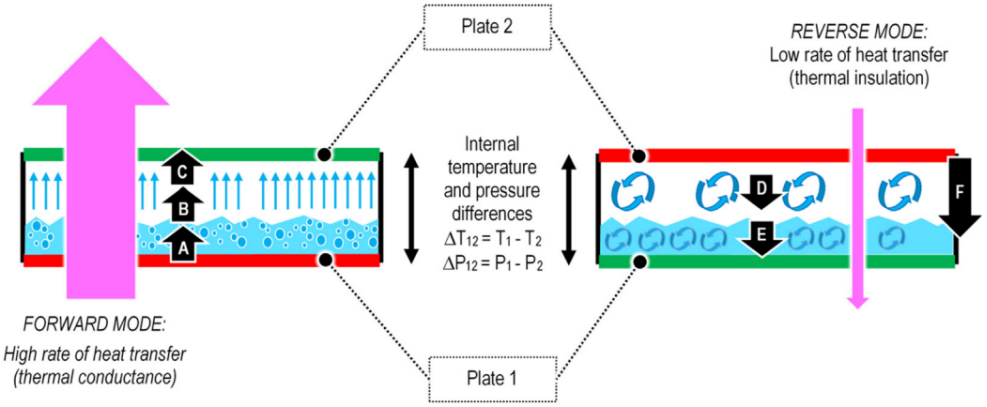


FIGURE 2.8: Heat transfer mechanisms in a Planar Liquid-Vapour Thermal Diode. Adapted from [33].

Finally, we have **radiation TDs**. Typically, such devices are made of two blocks of different materials separated by a nano-scale vacuum gap (Fig. 2.9(a)), and they are the main stream thermal rectification devices for nanoscale applications. Thermal radiation is the dominant heat transport mechanism in these components, and can be described as random thermal currents in an object that generate electromagnetic waves with a characteristic wavelength, i.e., it consists in the emission of internal energy of that object [39, 40].

This way, in this type of thermal diodes, one defines the forward direction as the case where heat is transferring, through thermal radiation, from the emitter to the receiver, where the first emits radiation and the second absorbs it.

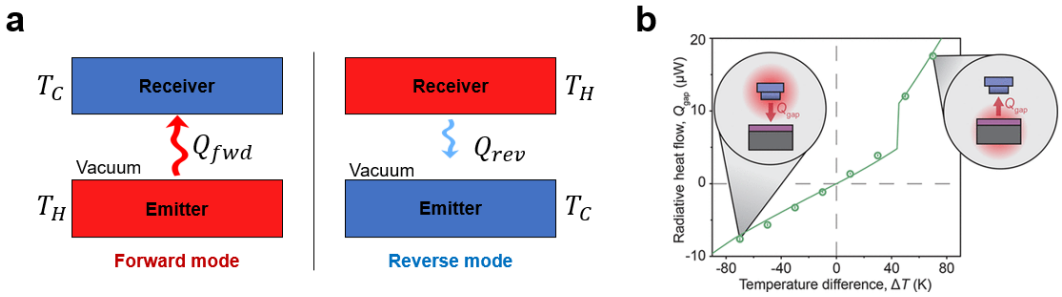


FIGURE 2.9: **(a)** Schematic representation of a radiative TD. **(b)** Transfer function obtained for a PCM-based radiative TD. Adapted from [36].

As indicated in Fig. 2.6, PCMs, non-PCMs, and superconductors are three of the main material groups used in radiative TDs. The emissivity of **Phase change materials** changes after the occurrence of a phase transition [8]. Thus, an accurate choice of PCMs to incorporate in a radiative TD allows the manipulation of the desired emissivity difference between the forward and reverse direction, so that thermal rectification between the emitter and receiver is possible. Among the suitable PCMs for this type of applications, vanadium dioxide ($VO_2$) is a very popular material due to its metallic-to-insulating state transition [41], and several computational and experimental studies have been performed with this material [42–45]. Fig. 2.9(a) shows the transfer function of a study done with a $VO_2$ based radiative TD, where the plotted transfer function clearly shows a rectification behavior. A few examples of diodes that used this type of materials are indicated in table 2.1.

Even with the advantages of PCM materials that were mentioned, it is possible to use **non-PCM materials** for thermal rectification in radiative diodes. A common approach is to modify the optical properties of materials trough doping techniques. Various studies have used emitter and receiver layers made of **silicon** with different levels of doping and either in the form of bulk, thin film, or both, where the thickness of the vacuum gap and the asymmetric dielectric function of silicon are variables that massively affect the heat transfer [46–48]. As to the case of **superconductors**, the change in their therm-optical properties, including a massive increase in reflectance, after surpassing phase transition temperatures makes them interesting materials for radiative TDs [38, 49]. Since superconductors have really low critical temperatures, these TDs can be implemented in extremely

cold environments. Table 2.1 includes the thermal rectification ratios obtained in a few studies of this type of devices.

#### 2.1.3.3 Applications

In the previous section, several thermal rectification mechanisms of different types of TDs were discussed, so now we shall introduce a couple of applications of these devices and the advantages they bring to a thermal management system.

On of the most notable use-cases of TDs is related to **thermoelectric power generation systems**. When using solar energy to generate electricity, there are two main methods that are used for the energy conversion [50]. One method is to use photovoltaics (PVs) that transform radiation directly into electricity, and the other is to utilize solar thermal energy. However, solar energy systems present some flaws, one of them being the inability to generate electricity during nigh-time. So far, this drawback has been addressed through storage of the excess electricity that is harvested during the day and further release during nigh-time [51]. This solution still has some limitations, including the extra space for the storage system and energy dissipation that occurs during the storing and releasing processes, which end up compromising the efficiency. To tackle these problems, a few authors have already proposed systems where **TDs** and thermal storage units are combined in order to achieve 24-hour solar electricity generation [52, 53]. In figures 2.10(a) and 2.10(b) we have illustrated a comparison between a conventional and a 24-hour electricity generation system that uses a TD bridge, respectively.

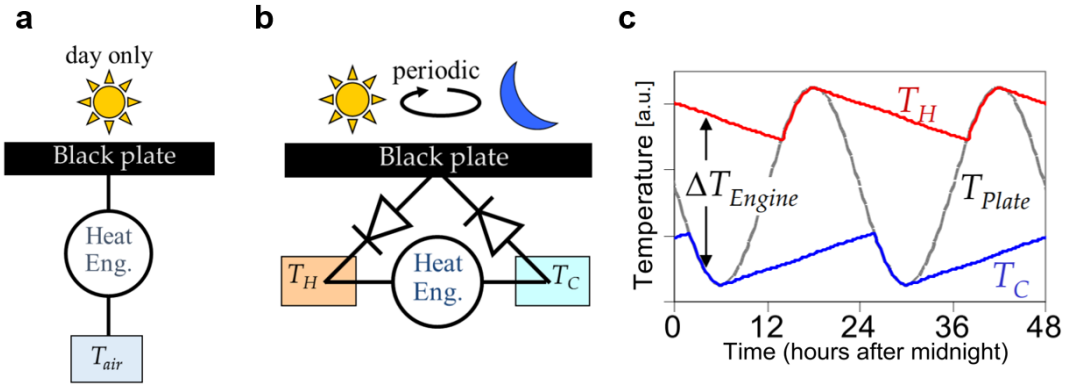


FIGURE 2.10: **(a)** Thermal power generation during daytime only. **(b)** Basic structure of a TD bridge for continuous solar energy harvesting. **(c)** Conversion of oscillating temperatures into almost-constant temperatures. Adapted from [52–54].

A TD bridge circuit is a kind of thermal circuit that is able to convert daily temperature oscillations into a single polarity temperature gradient [8]. Since a TD can manipulate

heat flux, the $\Delta T$ across the output device is maintained in a single direction. Therefore, a TD bridge circuit can be helpful for power generation systems under an alternating energy condition, which in the case of solar energy systems corresponds to the alternation between hot temperatures during the day and cold temperatures during the night (Fig. 2.10(c)).

Pivoting towards the application of TDs in **caloric refrigeration systems**, one should start by mentioning that indoor cooling corresponds, at global level, to almost 20% of energy consumption in buildings [55]. Among the many existing types of cooling systems, vapor compression refrigeration (VPR) has become standard in the industry due to its maturity and low cost. Nevertheless, these systems have considerable effects on ozone depletion and, consequently, global warming [8]. As a result, a lot of effort has been put into the development of alternative cooling solutions. From the systems that were already tested, magnetocaloric (MC) refrigeration is on the verge of competing with VPR, due to the latest development breakthroughs on magnetocaloric materials (MCMs) and design concepts of these systems [56]. MC refrigeration belongs to the group of caloric refrigeration systems, i.e., refrigeration systems that implement caloric materials for heat absorption or dissipation. In turn, caloric materials are materials that thermally respond to an external trigger: their temperature can be changed through the presence/absence of a magnetic field, in the case of MC refrigeration, electric field, pressure, etc [57]. Fig. 2.11(a) provides a schematic diagram of the thermodynamic cycle in a refrigeration system.

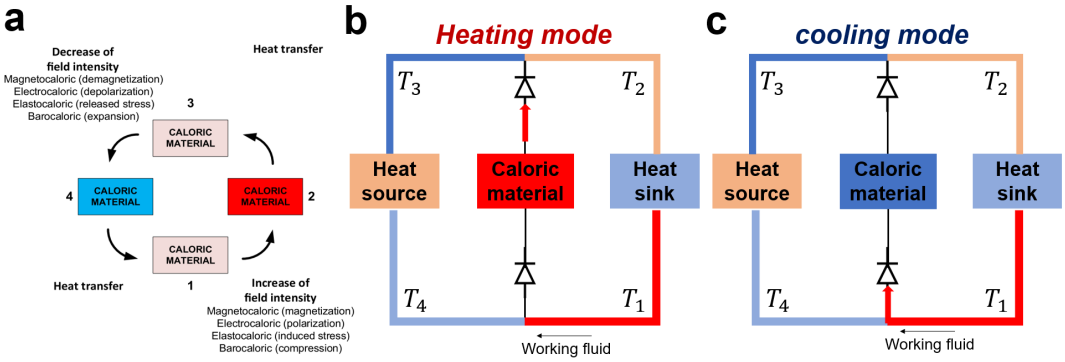


FIGURE 2.11: **(a)** Illustration of the operation processes of caloric refrigeration systems. Schematic diagram of a caloric refrigeration system with thermal diodes when the caloric material is under **(b)** the hot state and **(c)** the cold state. Adapted from [58].

The typical way of establishing a caloric refrigeration system is to circulate a working fluid between the heat source, heat sink, and caloric materials for heat transfer to occur.

The main issue of this strategy has to do with the oscillation of the fluid, i.e., the fluid is not in direct contact with all the components, which affects the heat exchange and efficiency of the system [59]. Using a TD is one of the possible solutions for this problem (Figs. 2.11(b) and (c)). Placing the thermal diodes on the top and bottom of the caloric material, and given the orientation of its forward direction, makes the fluid flow in only one direction, facilitating the heat exchange process [60]. This way, the implementation of this components in caloric refrigeration systems can improve both the operating frequency and the coefficient of performance (COP).

## 2.2 Phase change materials for thermal management

As mentioned in the previous chapter, society is currently in an urge to develop innovative materials and devices that provide a sustainable contribution to an efficient use of waste heat and improvement of thermal energy systems [61]. In this area, a class of materials that has gained a significant attraction are the so-called **phase change materials (PCMs)**. These are materials that have a high enthalpy, which means they are able to, in small volumes, absorb and release large amounts of energy in the form of latent heat at solidification and melting stages, respectively. Using PCMs for **thermal energy storage** (TES), not only opens an elegant and realistic path towards a more efficient storage, but also allows previously wasted energy to be used in domestic and industrial sectors [62].

The following sections present some theoretical background of PCMs in the context of thermal management, the main types of PCMs that have been developed so far and their respective applications. The final section is dedicated to PCM-based thermal diodes.

### 2.2.1 Methods of TES with PCMs

Storing thermal energy can be done by cooling, heating or, in the specific case of PCMS, by melting, solidifying, or vaporizing a material, where energy becomes available as heat when the process is reversed. There are two methods through which TES can occur: sensible heat thermal energy storage (SHTES) and latent heat thermal energy storage (LHTES).

In the case of **sensible heat storage**, thermal energy can be stored by raising the temperature of a solid or liquid, and its efficiency depends on how the material's specific heat ($C_p$) changes during the process. The amount of stored heat, $Q$ (J), is then given by

$$Q = \int_{T_i}^{T_f} mC_p dT, \tag{2.3}$$

where $m$ is the mass of the heat storage medium (kg), $T_i$ and $T_f$ are the initial and final temperatures ($^o$ C) [63]. The materials can store heat trough the previously discussed heat transfer mechanisms: conduction, convection and radiation. A typically used material for SHTES is water (in the liquid state), due to its low cost and high $C_p$ [64].

However, **latent heat storage** (LHS) is considered to be a more efficient method for TES. In this mechanism, the storage material absorbs or releases heat as it undergoes a phase transition: solid to solid, solid to liquid and liquid to gas, or the other way around. A PCM-based LHS system has a storage capacity given by

$$Q = \int_{T_i}^{T_m} mC_p dT + ma_m \Delta H_m + \int_{T_m}^{T_f} mC_p dT, \tag{2.4}$$

where $a_m$ is the melted fraction and $\Delta H_m$ (J/kg) is the heat of melting per unit of mass [63].

Thermal energy systems based on latent heat management have a far superior storage density and are gifted with a narrower range of temperature between storing and releasing heat, when compared to sensible heat systems [65]. Taking this into account, researchers have come up with a number of criteria that an **ideal PCM** should meet in order to be implemented in thermal management systems. These criteria, listed in table 2.2, make reference to thermal, physical, chemical and kinetic properties [66–68].

| **Properties** | **Criteria** |
|---|---|
| Thermal | melting temperature in the desired operating range |
| | high phase transition latent heat per unit volume |
| | high specific heat, to provide significant additional SHS |
| | high thermal conductivity of both phases |
| Physical | small volume change on phase transformation |
| | low vapor pressure at the operating temperature |
| | favorable phase equilibrium |
| | congruent melting of the PCM |
| | high density |
| Kinetic | no supercooling |
| | high nucleation rate |
| | adequate rate of crystallization |
| Chemical | long-term chemical stability |
| | completely reversible freeze/melt cycle |
| | compatibility with the construction materials |
| | no corrosion influence on the construction materials |
| | non-toxic, non-flammable and non-explosive |

TABLE 2.2: Set of criteria that a PCM for TES must fulfill.

Alongside these properties, a PCM ideal for thermal applications must be available in large amounts and have a low cost [66–68]. Unfortunately, in reality those conditions do not hold for the majority of PCMs. On the other hand, in recent years the design and characterization of new materials for energy storage has taken a major step forward not only in terms of performance but also durability [66].

### 2.2.2 Classification of PCMs

In a recent past, there were several classes of materials that were pointed out as potential PCMs such as hydrated salts, paraffin, fatty acids, polymers and eutectics of both organic and non-organic compounds. PCMs can be split into three main categories, according to the temperature range over which the phase transition being used for TES occurs ($T_{pt}$) [69]:

1. Low temperature PCMs $\rightarrow T_{pt} < 15$ ºC - air conditioning and food industry;
2. Mid temperature PCMs $\rightarrow 15 < T_{pt} < 90$ ºC - solar, medical and electronic applications (most popular);
3. High temperature PCMs $\rightarrow T_{pt} > 90$ ºC - industrial and aerospace applications.

Moreover, PCMs can also be classified by the type of their phase transition, where we can have: gas-liquid, solid-gas, solid-liquid and solid-solid systems. Fig. 2.12 indicates the commonly used types of PCM materials for the various phase transition modes, as well as typical and conventional materials for SHS systems.

Solid-gas and liquid-gas PCMs have very limited applications in thermal management systems due to the large volume expansions that occur in the transition phase, which is the opposite case of solid-solid and solid-liquid transformations. Hence, from an economical and practical standpoint, solid-solid and solid-liquid PCMs are more attractive for TES systems. It is worth noticing that, despite solid-solid PCMs having a generally lower latent heat than solid-liquid PCMs, using the former group tackles the issue of material leakage at temperatures above $T_{pt}$ that happens in solid-liquid PCMs [71].

### 2.2.3 Applications of PCMs

After making reference to the novel thermal properties of phase change materials and presenting their main categories, it is now convenient to mention a few applications. PCMs

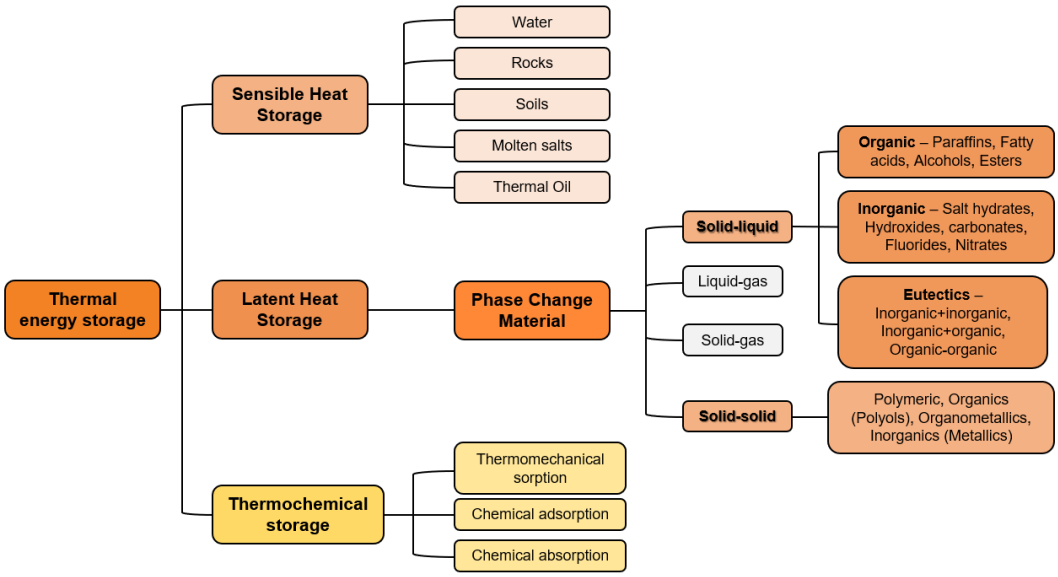


FIGURE 2.12: Diagram of the different groups of commonly used materials for thermal storage methods. Adapted from [70].

are implemented in a wide range of scenarios: from the building industry and textiles to solar energy systems and automobiles. More recently, the number of applications has dramatically increased, especially in the areas of electronics and medicine [61]. In the next paragraph a couple of examples of these applications are presented

Due to the price increase and environmental concerns around fossil fuels, the development of innovative energy storage systems for **heating and cooling in buildings** has become a hot research topic. In extremely cold or hot environments, the consumption of electricity during day and night is very different, and this happens because the need for domestic heating or cooling also varies in the same 24-hour period [72]. Studies of PCM-based passive and active storage systems have shown to be a promising solution to reduce these consumption variations. For example, Shilei et al. studied impregnation of wallboard with a PCM material (eutectic mixtures of CA and LA) as a possible strategy to increase the efficiency of indoor temperature moderation [73](Fig. 2.13).

In the field of **electronics**, the fast-paced evolution of devices with reduced form factors has resulted in a tremendous need for thermal management systems efficient enough not to compromise the performance of devices such as cellphones, laptops and digital cameras [61]. Since these devices are typically operated for long periods of time, PCM based cooling systems come to the scene as viable alternative to other passive cooling techniques, such as copper or aluminum heat sinks. On this note, it was realized that a heat sink based on PCMs could be capable of maintaining the temperature of electronic

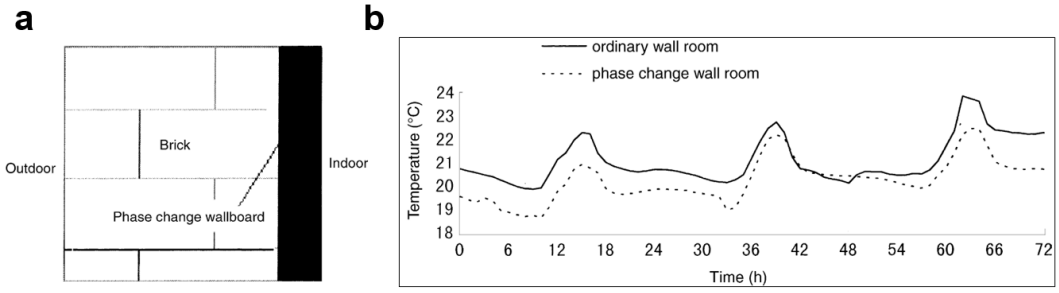


FIGURE 2.13: **(a)** Structure of phase change wall. **(b)** Indoor temperature variation curves for a 3-day period. Adapted from [73].

devices below the critical level. In fact, it was already demonstrated that filling the cavities of heat sinks with a PCM, as illustrated in fig. 2.14, enhances the cooling performance of the system when compared to a conventional heat sink [74].

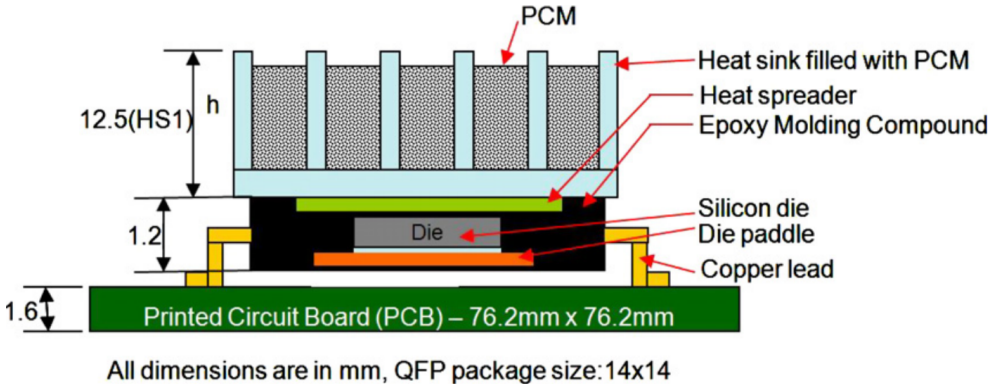


FIGURE 2.14: Schematic representation of the cross-section of a PCM filled heat sink placed on a quad flat package. Adapted from [74].

### 2.2.4 PCMs for thermal rectification

In section 2.1.3.1 it was mentioned that one of the criteria for thermal rectification is the use of materials with strongly temperature-dependent thermal conductivities, which, unfortunately, is extremely rare in nature. This is where phase change materials, which can exist in two states with distinct thermal conductivities, provide a unique opportunity to build systems able to realize nonlinear thermal transport.

It was found and verified by Dames an analytical expression that estimates thermal rectification ratios for TDs made of two materials with properties that have a different dependence on thermal conductivity [11]. It was claimed that the difference in temperature-dependent thermal conductivities, the thermal resistance between the two materials and

the temperature gradients were all factor that conditioned the occurrence of thermal rectification. In conclusion, this study proved that it is possible to observe thermal rectification by combining either a PCM and a non-PCM, or two PCMs with different $T$-dependent thermal conductivities. This way, a whole world of possibilities for PCM-based TDs is open.

Giving an example of a possible TD structure that includes PCM materials, figure 2.14(a) includes an illustration of the measuring setup that Chen et al. [14] used to investigate (numerically and experimentally) a thermal rectifier made of two PCMs: eicosane and Polyethylene glycol, which have different solid-liquid phase transition temperatures. The results of this study also indicated that both the amount of PCM used in the sample (fig. 2.15(b)) and the temperature of the heater influences the thermal rectification ratio, where one can see that an increase in PCM content leads to a more detectable rectification effect.

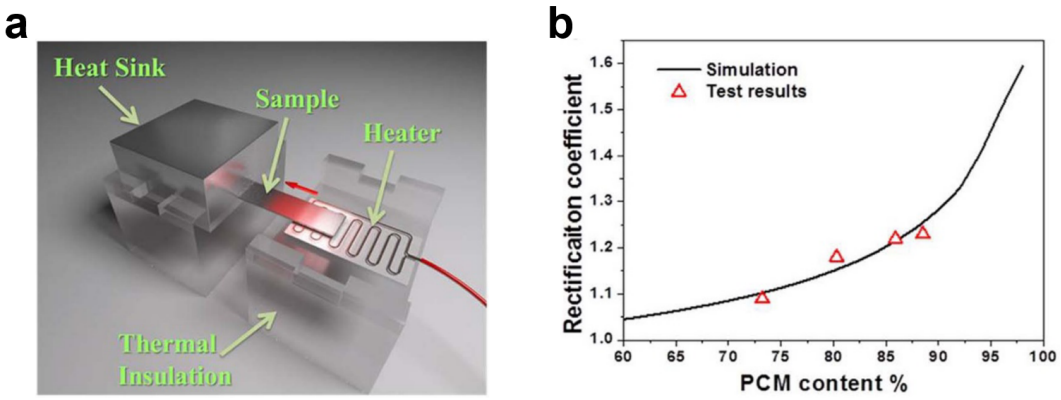


FIGURE 2.15: **(a)** Schematic of the experimental setup to measure the thermal rectification of the PCM-based thermal diode. **(b)** Effect of the amount of PCM content on the thermal rectification ratio of the TD. Adapted from [14].

# Chapter 3

# Designing and simulating a 2D PCM-based Thermal Diode

As mentioned before (section 1), the main goal of this dissertation was to design and numerically simulate a **two-dimensional device that showcased thermal rectification**. For this purpose, our choice was to, after conceiving a structure that met the criteria mentioned in the previous chapter and selecting adequate materials, compute the heat transfer phenomena in a Python framework called *heatrapy* and then compare the results for the forward and reverse modes and infer whether thermal rectification was present or not. The following sections cover not only the thought process of designing the TD (geometry and materials) and methods used for the simulations, but also some initial results and respective discussion.

## 3.1 Designing a two-dimensional TD using PCMs

The primary guidelines that a thermal diode must follow in order to showcase thermal rectification are already delineated in section 2.1.3.1. To meet these requirements, one has to not only carefully select the set of materials to use in the device but also come up with a well-thought-out geometric design.

Before specifying the materials that were selected and cover the technical details of the numeric simulations, a more comprehensive overview of the device's mechanisms must be given. As covered in the preceding chapter, a TD is a device that has a preferential heat conduction direction, corresponding to the *forward* configuration. In light of this, we propose a structure (Fig. 3.1) that takes advantage of the thermal properties of PCMs

paired with other materials, which, theoretically, may result in asymmetric heat flow and lead to the occurrence of thermal rectification [11].

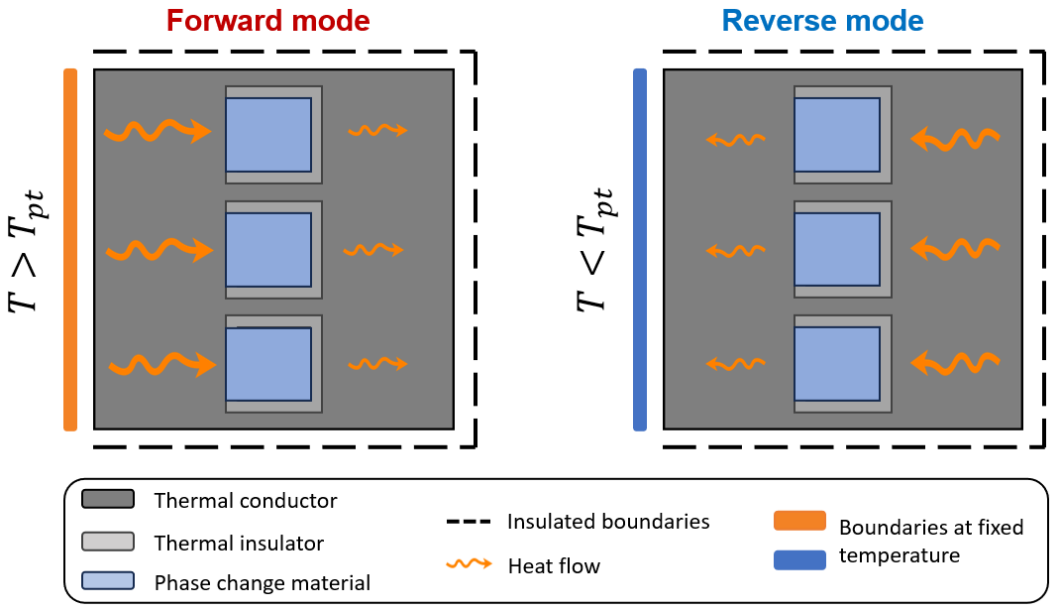


FIGURE 3.1: Schematic representation of forward and reverse modes for the conceptualized 2D PCM-based thermal diode to be simulated.

Figure 3.1 includes the structure and boundary conditions of the thermal diode, and illustrates the working principle for both *forward* and *reverse*, which intends to highlight the expected difference in heat flow between the two cases. To achieve this, and recalling the criteria for asymmetric heat flow, we decided to include **three different types of materials** confined to different shapes, each with a different role:

- **Thermal conductor** - having a high thermal conductivity, results in high heat flow rates across the device (aluminum (Al), Copper (Cu) and Silver (Ag) are examples of good thermal conductors, often employed in heat sinks for thermal dissipation). In this case, we opted for a square-shaped block with three thermally insulated sides and a fourth side (left) that is subject to a fixed temperature.

- **Phase change material** - when heated above a critical temperature, its physical state changes and the thermal conductivity changes with it, contributing to a nonlinear heat flow (examples in section 2.2.2). Our device includes three square-shaped spots of PCM vertically spread out across the medium axis. This way, there is still heat flow through the thermal conductor spaces in between and, until the phase transitions occurs, thermal energy is stored in the PCM;

- **Thermal insulator** - having a really low thermal conductivity (vacuum being the ideal), three "C-shaped" thermal insulating components surrounding the PCM have the role of preventing direct heat flow between the PCM and the thermal conductor. As illustrated in Fig. 3.1, the thermal insulator only allows heat exchange between the PCM and the thermal conductor on one side of the PCM spots. Additionally, due to the geometric orientation of this component, the heat flow on this "open side" starts faster in the case of the *forward* mode. Without this component, the device would be totally symmetrical, and its performance would be invariant to the direction of heat flow.

Regarding the mentioned boundary conditions of the system, firstly, one opted for thermally insulating three sides of the device to provide a more unidirectional heat flow and potentially highlight the heat flow differences between the two possible configurations. Secondly, the remaining side of the device is at a fixed temperature, which dictates the direction of heat flow: in the case of the *forward* mode, that temperature is higher than the phase transition temperature ($T_{pt}$) of the PCM and lower for the *reverse* mode. Such conditions are imposed due to the fact that the whole system is initially at a temperature ($T_{glob.}$) that is slightly lower than $T_{pt}$, meaning that the device only goes through the phase transition in the *forward* configuration.

## 3.2 Validation of the rectification behavior

Now that we covered the generalized version of the TD structured that is intended to be simulated, one must discuss the materials that were selected and numerical models that were implemented. For a preliminary scenario, one decided to use Aluminum, vacuum and water for the thermal conductor, thermal insulator, and PCM, respectively. The reasons for this selection are the following:

- **Aluminum** - Has a high thermal conductivity (237 W/m·K) and is a commonly used material in thermal management systems that involve thermal dissipation;
- **Vacuum** - Is the ideal thermal insulator (null thermal conductivity), despite not being the most practical solution for real-life applications.
- **Water** - It is a simple and well-known PCM that has its solid-liquid phase transition at 0 ºC, making it suitable for both cooling and heating applications. Moreover, it has

a relatively high heat of fusion*, meaning it is able to store a considerable amount of thermal energy during phase transition.

Now that one has gone through the materials, geometry, and working principles of the idealized TD, the details of the numerical simulations must be addressed. The goal, as explained earlier, is to compute the heat flow for both *forward* and *reverse* configurations, which correspond to different temperature biases at the left boundary of the system. For these simulations, the Python framework *heatrapy*, developed by Silva et al. was used [75]. For a given 2D structure, denoted as a `thermal object`, with specified materials, spacial and time steps, and temperature boundary conditions, this framework is able to compute heat transfer phenomena for the desired period of time by computing the 2D heat equation, as it is fully described in appendix A.

Figure 3.2 includes a scheme of the *heatrapy* thermal objects after providing the previously mentioned materials, discretization parameters, and boundary conditions as an input. We opted for a 12x12 $cm^2$ system divided into a mesh of 61x61 points with a side of 0.2 cm $(dx, dy)$. The ambient temperature of the system was set at 272.9 K (0.1 K below the solid-liquid $T_{pt}$ of water). After this, the `compute` function was used to calculate the heat transfer phenomena across the whole for a period of 30000 s ($\sim$ 8 hours), which returns the temperature every second for each point. An example of the Python code written for the simulations is provided in appendix B.

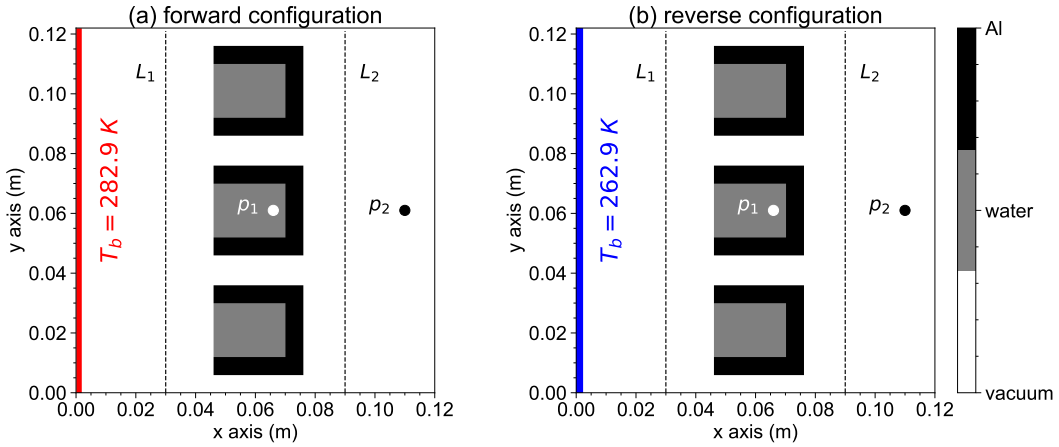


FIGURE 3.2: Schematic representation of the *heatrapy* thermal objects used for simulating the **(a)** forward and **(b)** reverse modes. $P_1$, $P_2$, $L_1$ and $L_2$ indicate regions of interest to evaluate temperature and heat flow. In the materials legend, 'Al' stands for Aluminum.

*energy required to go from solid to liquid state

In the following sections, we present a comprehensive analysis of the conducted simulations. Furthermore, we outline a few modifications that were made in order to compute the device's thermal rectification ratio and transfer function.

### 3.2.1 Results

Before computing heat transfer rates and rectification ratios, one must verify if there are any differences in the temperature curves of the *forward* and *reverse* modes, measured at critical points of the device. This way, as indicated in Fig. 3.2, one shall investigate the temporal evolution of temperature at $P_1$, in the middle of the central PCM spot, and $P_2$, a point in the aluminum block located to the right of the insulated PCM spots.

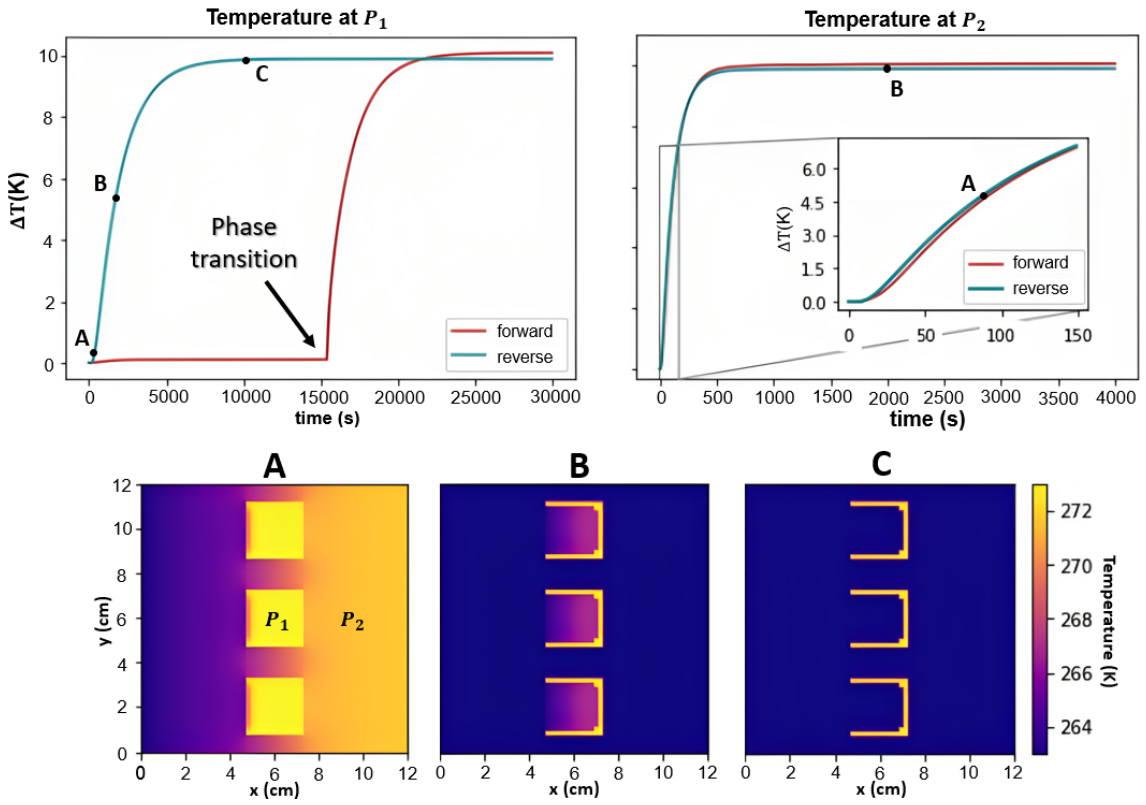


FIGURE 3.3: **Top -** Temperature variation curves over time measured at the critical points $P_1$ and $P_2$ for both configurations. **Bottom -** Temperature heat maps at relevant timestamps for the reverse mode.

The curves in the plots at the top of Fig. 3.3 represent the temperature variations (in absolute value) at the critical points mentioned. From the left, one can see that in the *forward* configuration, the water temperature ($P_1$) is held constant for almost half the duration of the simulation, meaning the phase transition is yet to occur, which finally occurs after approximately 4 hours. In turn, for the *reverse* mode, the temperature starts

decreasing right away* (due to the -10 K temperature difference fixed at the left boundary that imposes a heat flow from the right to the left) and reaches a constant value around the three-hour mark time. The plot on the right side shows the temperature variation measured at a point on the aluminum, and, as expected, one can see that the curves for the *forward* and *reverse* modes are almost identical due to the aluminum's high thermal conductivity. From these results, we can already infer that the heat flow rates will have a different spatial dependency for the two configurations.

Having access to the temperature of each point over time $T_x^y(t)$, it is possible to compute the thermal power density, $P$ (W/m). This quantity measures the device's ability to conduct heat by quantifying the rate at which heat flows through a material per unit length. In Dig. 3.2 we have identified two vertical cross sections (perpendicular to the heat flow direction) where one intends to measure the thermal power. Since the *heatrapy* thermal object consists of a 61x61 two-dimensional array, one can compute the thermal power density over a certain line $L_1$ as follows:

$$P_{L_1}(t) = -k \sum_{i=1}^{61} \frac{T^i_{x_{L_1+1}}(t) - T^i_{x_{L_1-1}}(t)}{dx}, \tag{3.1}$$

where $k$ is the thermal conductivity of the material that covers the region we want to study (aluminum in this case). The fraction numerator is the temperature difference between two consecutive points in the horizontal direction, which becomes the temperature gradient when divided by the spatial step $dx$. Then, the sum of the gradients in the vertical direction is computed. The results obtained are represented in Fig. 3.4.

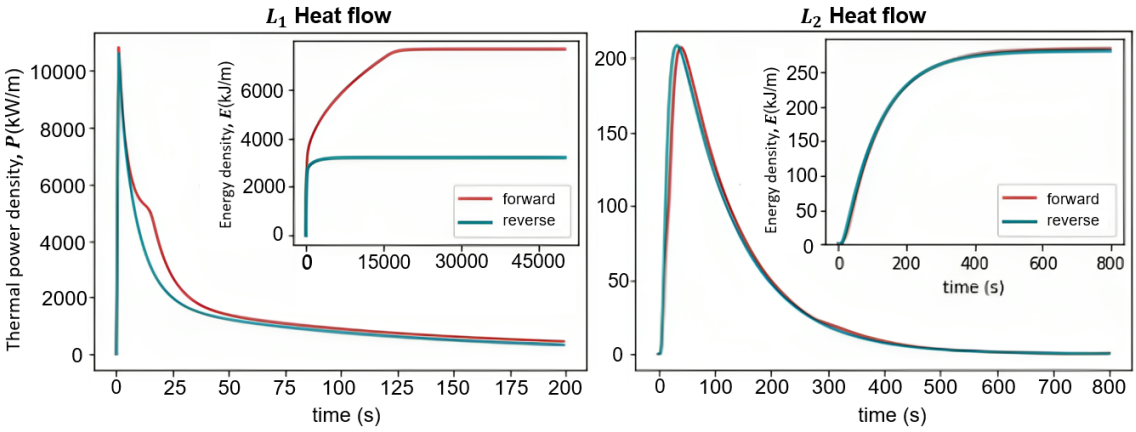


FIGURE 3.4: Thermal power and total energy density time curves measured across the regions $L_1$ and $L_2$.

*the graph shows an increase in temperature variation because we are taking its absolute value for comparison purposes between the two modes.

From the plots, one can see that in the first minutes of the simulations, the heat flow rate measured at $L_1$ is drastically higher than in $L_2$, and a maximum thermal power density value (>10 MW/m) is reached, which can be explained by its proximity to the left boundary of the system where the fixed triggering temperature is imposed. As the system enters thermal equilibrium (the whole system is at the same temperature), the thermal power across both regions goes to zero. However, despite the differences in temperature variation and heat flow rates mentioned so far, we cannot assume that thermal rectification is present. To tackle this, the total thermal energy density, $E$ (J/m), measured at the same critical regions must be calculated using:

$$E_{L_1}(t) = \int_0^t P_{L_1}(t')dt'. \tag{3.2}$$

In a two-dimensional device, this quantity measures the amount of energy stored or present in a certain area of space. In our specific case, one intends to measure the stored thermal energy at the $L_1$ and $L_2$ lines, which consist of arrays of 61 points with a thickness of 0.2 cm, meaning they can be interpreted as 2D areas. As the thermal power density across these same regions is already calculated, the stored thermal energy is obtained through the cumulative sum over time ($\int_0^t$). In the inset plots of Fig. 3.4 one can see the obtained results in the two configurations for each region. For the $L_1$ region, there is an evident difference in the thermal energy curves for the *forward* and *reverse* modes. We can see that, for the former configuration, the energy density reaches a value close to 8 MJ/m, which is more than three times higher than the energy stored for the reverse configuration. This is the main result that shows evidence of a preferential heat flow direction and an asymmetric thermal energy storage process. Regarding the energy density measured in the $L_2$ region, there are no visible differences between the two modes, which was already the case for the thermal power density.

Now that we have evidence that the proposed structure fulfills the requirements for thermal rectification, one can calculate the thermal rectification ratio and evaluate its performance. However, this figure of merit cannot be calculated using the configuration illustrated in Fig. 3.2. In chapter 2 it was mentioned that a thermal diode is a two-terminal device with a fixed temperature in both terminals so that heat flows from the hot side to the cold side in a direction that corresponds to either the *forward* or the reverse configuration. In these simulations, only one of the sides of the structure is at a fixed temperature, while the other boundaries are insulated. In order to simulate the conceived structure

with the boundary conditions of a thermal diode (fixed temperatures on the left and right sides), a few modifications were made to the *heatrapy* thermal object and are illustrated in Fig. 3.5.

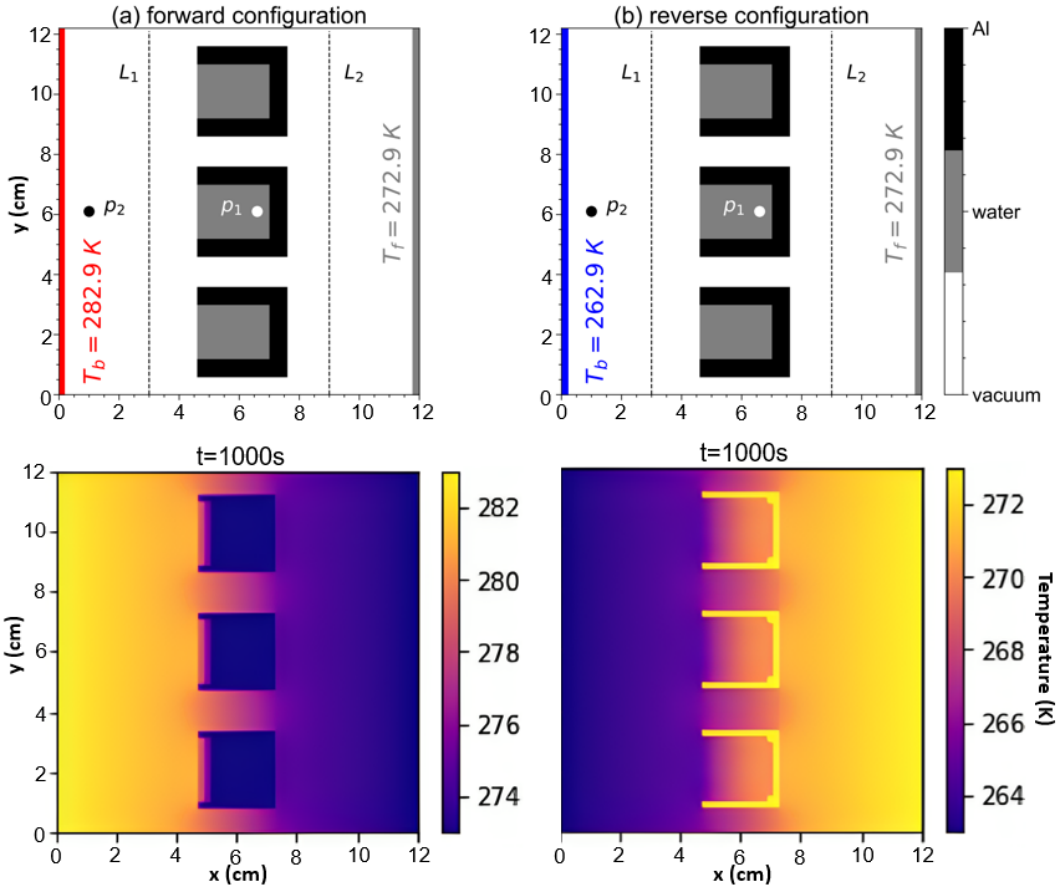


FIGURE 3.5: Modification of the *heatrapy* thermal object with a fixed temperature at right boundary for the calculation of the thermal rectification ratio and transfer function.

As one can see, the *forward* configuration corresponds to the case where the left boundary ($T_H$) is fixed 10K above the initial temperature (positive temperature bias) and the right boundary is held at that temperature ($T_C$), meaning that heat flows from the left to the right. On the other hand, the *reverse* mode happens when the left side is fixed 10 K below the initial temperature (negative temperature bias) and heat flows in the opposite direction. On the bottom of Fig. 3.5 we can see the heat maps for both configurations obtained at the t=1000 s mark time, which clearly shows an interaction between the heat flows imposed by the two boundaries, especially in the PCM regions.

The simulations were run in the same conditions (duration, time step, etc) and equations 3.1 and 3.2 were again used to compute the time curves for the thermal power density and total energy density, respectively. In fig. 3.6(a) we can see that the thermal power

density across $L_1$ has similar behavior to that obtained in the previous simulations, except that it is held constant for a long period of time before going to zero (inset plot).

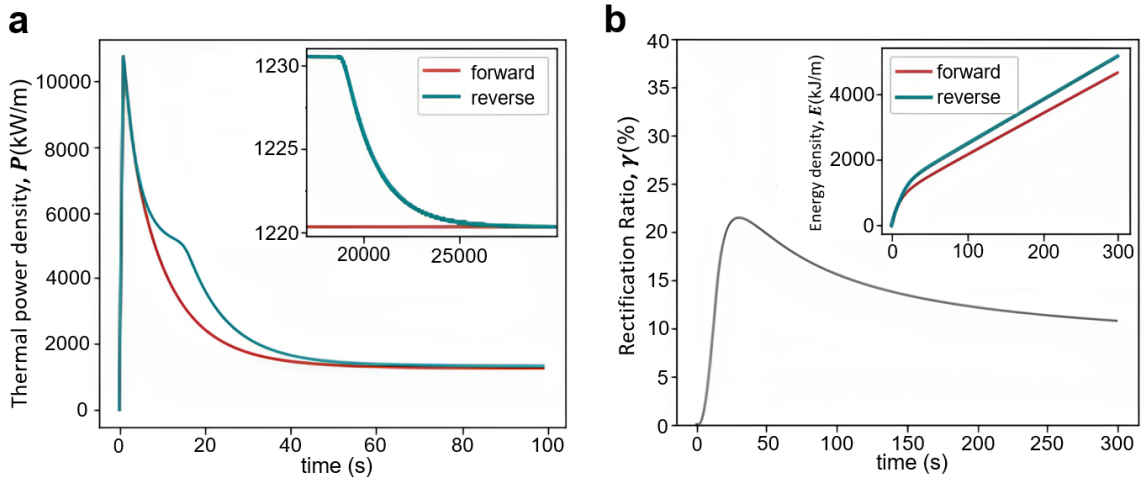


FIGURE 3.6: **(a)** Time evolution of the thermal power across $L_1$, **(b)** rectification ratio for a temperature bias of $\pm$10K, and total energy density (inset).

A slight reformulation of equation 2.2 was made to compute the thermal rectification ratio using the thermal energy density curves of the *forward* and *reverse* modes, that we already know how to calculate. Since the difference in stored thermal energy between the two configurations was observed for the $L_1$ region, $\gamma$ at this same region can be calculated as follows:

$$\gamma(\%) = \frac{E_{\text{forward}} - E_{\text{reverse}}}{E_{\text{reverse}}} \times 100\%. \tag{3.3}$$

From the results obtained, represented in figure 3.6(b), we can see that the rectification ratio increases as long as the difference between the energy densities of two modes also increases (inset plot), reaching a maximum value slightly above 20% and eventually going to zero. These results finally let us affirm that the initially proposed structure is in fact a thermal diode. However, we also mentioned that a convenient way of describing a non-linear thermal component is through its transfer function, a relation between a quantity that measures heat flow rate and temperature bias. For this purpose, the previous simulation was repeated for a set of 13 different values of triggering temperature ($\pm\Delta T$). In Fig. 3.7(a) we can see the rectification ratio curves obtained for each temperature, where it was noticed that the maximum $\gamma$ is inversely proportional to the module of the temperature bias.

As explained before, a negative temperature bias corresponds to the *reverse* configuration and a positive bias to the *forward* configuration. This way, a stable value of the

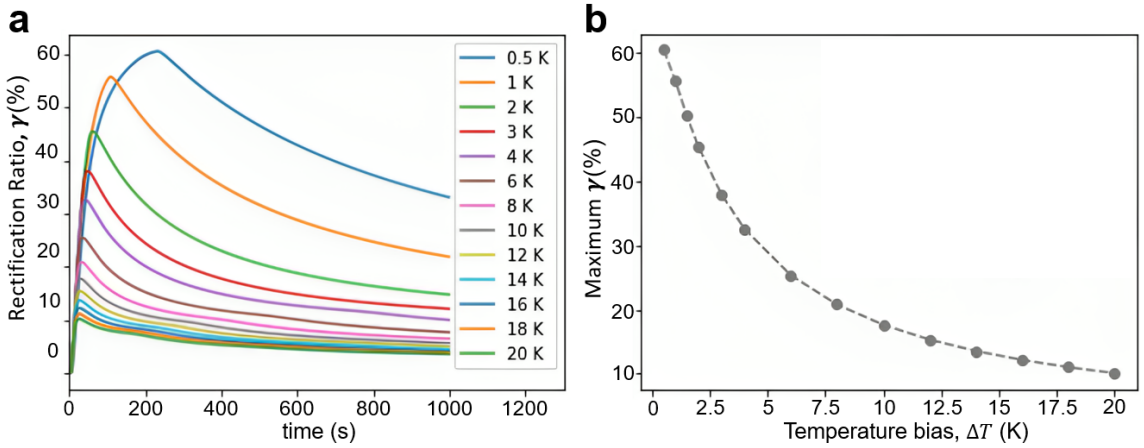


FIGURE 3.7: **(a)** Rectification ratio measured at $L_1$ for different values of temperature bias. **(b)** Maximum rectification ratio as a function of $\Delta T$.

thermal power density for each simulated case was plotted as a function of the respective temperature bias, resulting in the final transfer function (Fig. 3.8) of the idealized PCM-based TD. As intended, this result agrees with the nonlinear transfer function characteristic of thermal rectifiers (Fig. 2.1), especially for small triggering temperatures where the thermal rectification ratio is also higher.

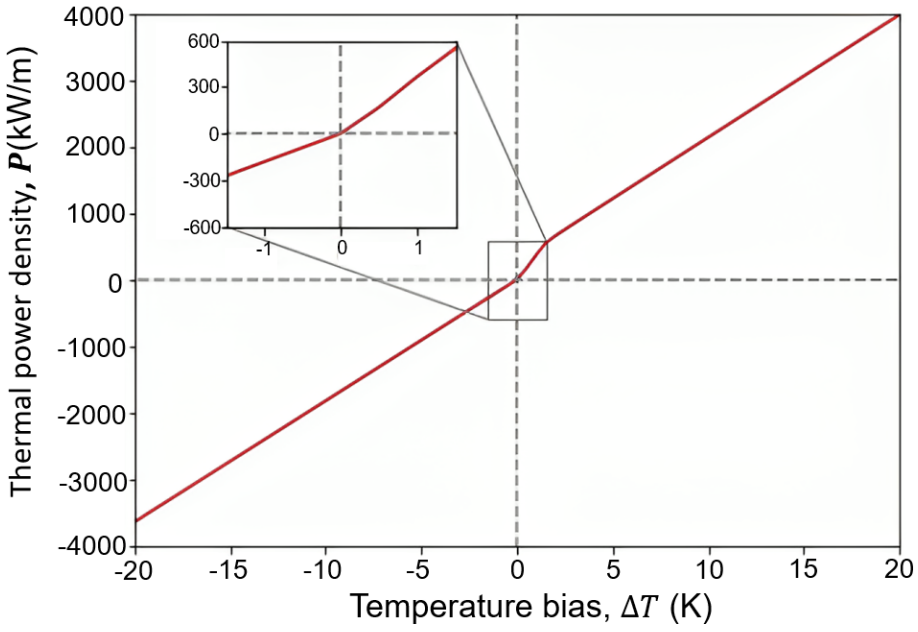


FIGURE 3.8: Transfer function of the TD: temperature dependence of converged thermal power density measured across $L_1$.

# Chapter 4

# Parameter tuning towards design optimization

In the previous chapter, we presented a proof-of-concept design for a two-dimensional thermal diode based on phase-change materials. We opted for a somewhat basic structure made of well-known materials: an aluminum square with three vertically aligned vacuum-insulated water spots. The results of the numerical simulations showed that the proposed device was able to act as a thermal rectifier. Now, in the following sections of this chapter, we will be taking a closer look at how different factors affect the performance of our design. A series of simulations to test various parameters was conducted with the aim of refining our concept and moving closer to building a physical prototype to be experimentally tested.

## 4.1 Influence of the thermal insulator

The first parameter that one must investigate has to do with the material used to thermally insulate the boundaries of the PCM. In the first simulations discussed in the last chapter, the material used for this purpose was vacuum, which is an ideal thermal insulator due to its null thermal conductivity. However, from a practical standpoint, it is not a viable option, especially considering the design and dimensions of our device. This way, a series of simulations testing the impact of using other materials for the device's thermal insulator role was conducted. In table 4.1 we list commonly used materials for thermal insulation that we tested and a corresponding set of relevant physical properties.

| **Material** | $k$ (W/m·K) | $\alpha$ (m$^2$/s)[1] | $C_p$ (J/Kg·K) | $\rho$ (Kg/m$^3$) |
|---|---|---|---|---|
| Acrylic | 0.19 | $1.23\times10^{-7}$ | 1470 | 1051 |
| Cellular glass | 0.041 | $3.57\times10^{-7}$ | 1000 | 115 |
| Cork | 0.039 | $1.08\times10^{-7}$ | 1900 | 190 |
| Extruded Polystyrene (XPS) | 0.034 | $7.56\times10^{-7}$ | 1500 | 30 |
| Polylactic Acid (PLA) | 0.13 | $5.82\times10^{-5}$ | 1800 | 1.24 |
| Silica Aerogel | 0.014 | $9.33\times10^{-8}$ | 1000 | 150 |
| Teflon | 0.25 | $1.15\times10^{-7}$ | 1000 | 2180 |

[1]Thermal diffusivity, $\alpha = \frac{k}{\rho C_p}$.

TABLE 4.1: Relevant physical properties of bulk materials tested as possible candidates for the thermal insulator role.

For this set of simulations, we used the same boundary conditions as the ones schematized in Fig. 3.2, where the only change was the thermal insulator. The goal was to verify if the difference in stored thermal energy between the *forward* and *reverse* configurations was still evident and then, based on these results, select a material that would be easy to machine if one were to build the device. The results obtained from these simulations are plotted in Fig. 4.1.

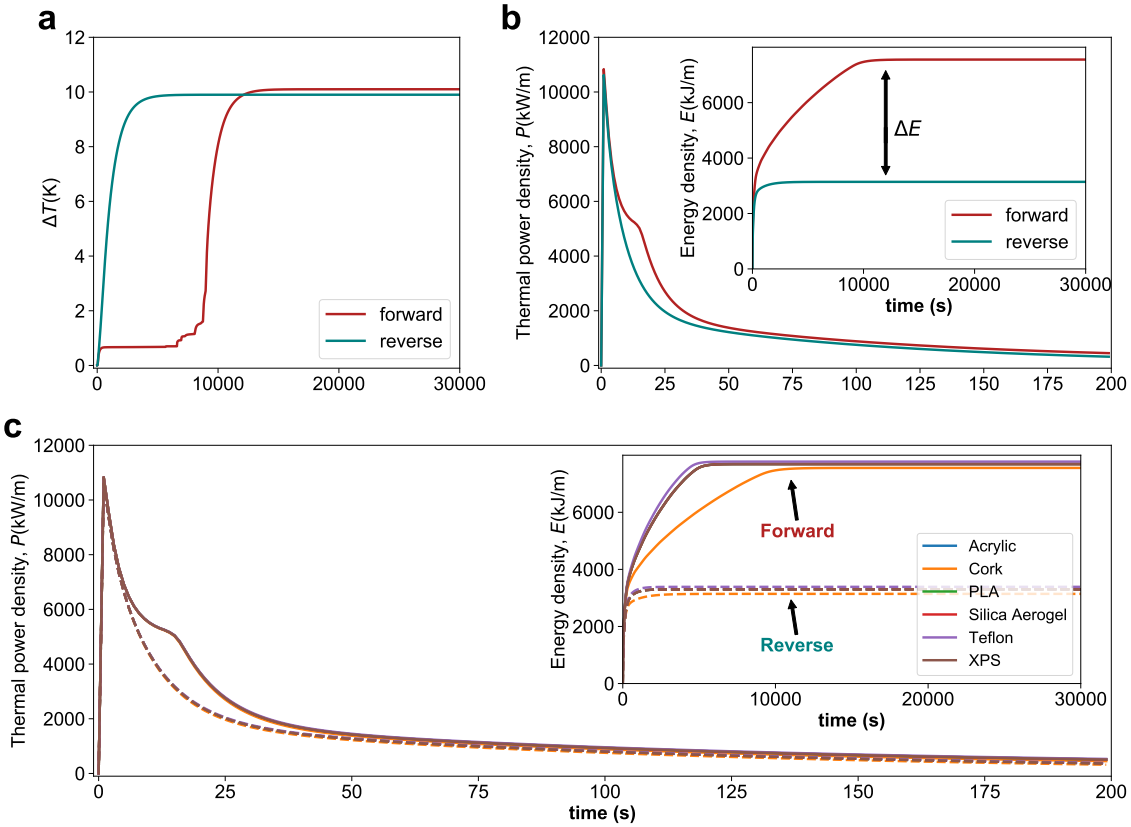


FIGURE 4.1: **(a)** Temperature variation curves measured at $P_1$ and **(b)** Power and energy (inset) densities measured at $L_1$ in the case where **cork** is used as thermal insulator. **(c)** Power and energy density (inset) curves obtained for all the tested materials.

As an example, in Figs. 4.1(a) and (b) we have the temperature variation curves, as well as the energy and power density curves, from the simulations where **cork** was used as the thermal insulator. The first plot clearly shows that, for the forward configuration, the water phase transition does not occur as suddenly as in the case of vacuum insulation. Regarding the difference in stored energy, the inset plot in figure 4.1(b) shows the intended difference in thermal energy density, $\Delta E$, between the two modes and leads to the conclusion that this material is a viable option for thermal insulation. After repeating this analysis for the remaining materials and obtaining the results presented in Fig. 4.1(c), we can conclude that all of them are capable of fulfilling the role of thermal insulator in our device. This way, other selection criteria more related to the practical side must come into play. In the end, **acrylic** came as a natural choice, mainly due to its robustness, price, availability, and the fact that it can be easily machined. In addition, acrylic is a commonly used material in applications where water resistance is desirable*, as it happens in this case. Therefore, from this point forward, the thermal insulator used in the simulations was acrylic.

## 4.2 Influence of geometrical parameters

Now that one was selected a more adequate set of materials to build the device, it is time to study the impact of geometrical parameters, such as shapes and sizes of regions occupied by the different materials, on the rectification performance. The influence of these parameters was analyzed through:

- **temperature variation curves for the *forward* configuration** - allows us to verify the impact on the time it takes to reach the phase transition instant;
- **maximum rectification ratio** - measures the impact of the varied parameters on the overall TD performance.

Recalling the previous chapter, the thermal rectification ratio is calculated using boundary conditions where a fixed temperature is imposed on both sides of the device, as illustrated in Fig. 3.5. The temperature and difference in energy density curves were obtained using the boundary conditions schematized in Fig. 3.2. In all simulations, we used a temperature bias of +10 ºC and -10 ºC for the *forward* and *reverse* modes, respectively.

*Acrylic can be considered a hydrophobic material, meaning it repels water to some extent. Materials like cork would easily soak in contact with water

### 4.2.1 Portion of PCM

The total amount of phase change material employed, or the proportion of the device's overall area that is taken up by PCM (% PCM), was the first parameter to be investigated in this set of simulations. To perform this study, one had to make a slight modification in the structure of the diode: instead of the three separate regions containing water used before, we opted for a single squared region, as schematized in Fig. 4.2(a). By increasing the area of the square, the percentage of PCM in the total area of device also increases. It is worth noticing that despite the change in the design, Figs. 4.2(b) and (c) still demonstrate the nonlinear temperature variation across the device due to the PCM presence.

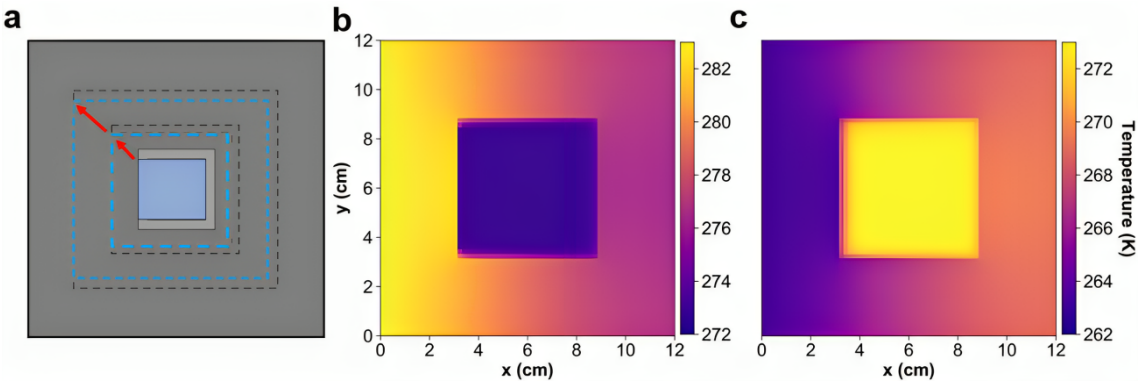


FIGURE 4.2: **(a)** Schematic representation of how the parameter of PCM amount was varied in the simulations. Heat maps for the **(b)** *forward* and **(c)** *reverse* obtained at the instant $t = 60$ s for a PCM amount ratio of 21%.

Firstly, we must look at the temperature variation curves in order to measure the impact of increasing the amount of PCM in the time it takes to reach the instant of the phase transition. Figure 4.3(a) includes the obtained results for the tested values of PCM%.

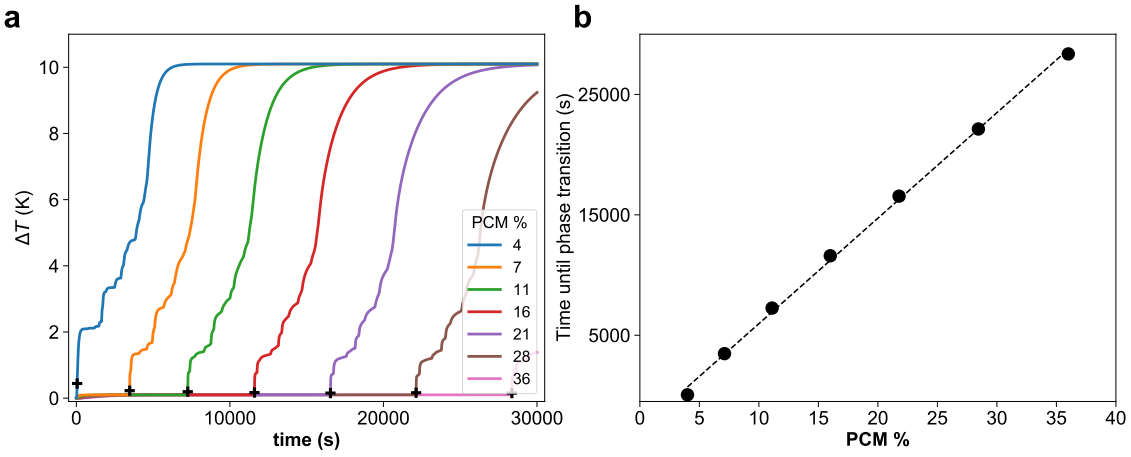


FIGURE 4.3: **(a)** Temperature variation curves, measured at $P_1$, for the *forward* mode for different amounts of PCM. **(b)** Time until phase transition as a function of PCM%.

It is clear that the more PCM is included in the thermal diode, the longer it takes to reach the phase transition instant and, as one can see in the plot of Fig. 4.4(b) a linear relation between these parameters was found. From these results one can also conclude that the the amount of PCM that is employed in a thermal diode is a quite limiting factor in terms of applications, since a large amount of material is translated into a slow actuation of the device.

Regarding the impact of the PCM % in the actual performance of the diode, one can see from the curves in the plot of Fig. 4.4(a) that rectifying behavior is heavily affected by the portion of used material. Plotting the maximum $\gamma$ for each case (Fig. 4.4(b)), we can see that it displays a quadratic relation with the amount of PCM, leading us to conclude that this parameter has a strong positive impact in the performance of the device, which agrees with the both numerical and experimental results obtained by Chen et al. [14]. It is worth pointing out that for a portion of PCM higher than 20% the rectification ratio surpasses the maximum value of 60% obtained in the initial simulations discussed in chapter 3.

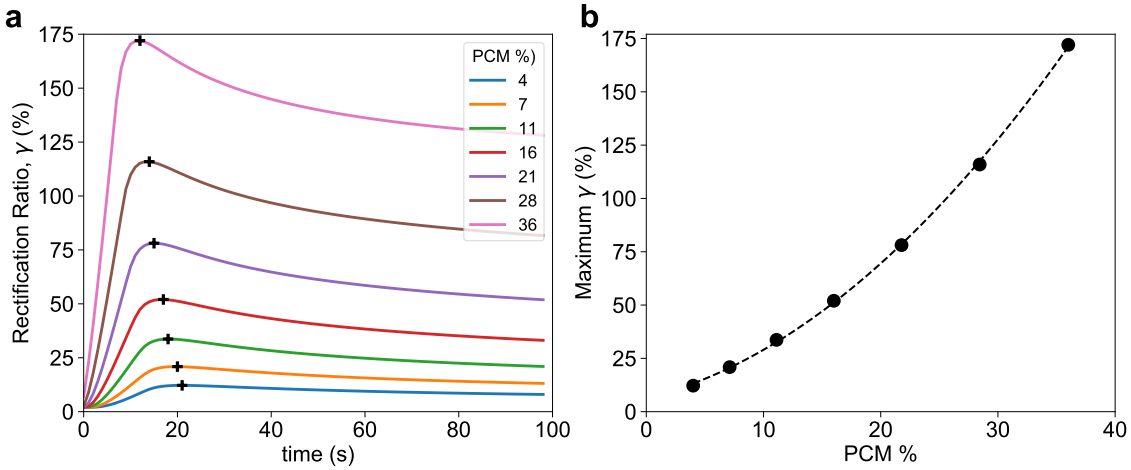


FIGURE 4.4: **(a)** Rectification ratio measured at $L_1$ for different amounts of PCM. **(b)** Maximum rectification ratio as a function of PCM amount percentage

### 4.2.2 Number and shape of PCM reservoirs

Besides demonstrating the importance of using an appropriate amount of PCM, the results from the previous section showed that geometrical modifications to the diode design are possible to implement without compromising its performance. Thus, one started looking at the possibility of not only testing the influence of the shape of the regions covered by PCM and thermal insulator, but also the number of sites that contain those materials. We ended up testing the impact of these parameters simultaneously by modifying

the structure to include a varying number of PCM regions with a circular shape, with the thermal insulator taking the form of semicircle shell. In Fig. 4.5 we have a schematic representation of how these changes in the device's structures were implemented in the `thermal object` to be simulated in *heatrapy*, as well as the heat maps for the case with two PCM regions.

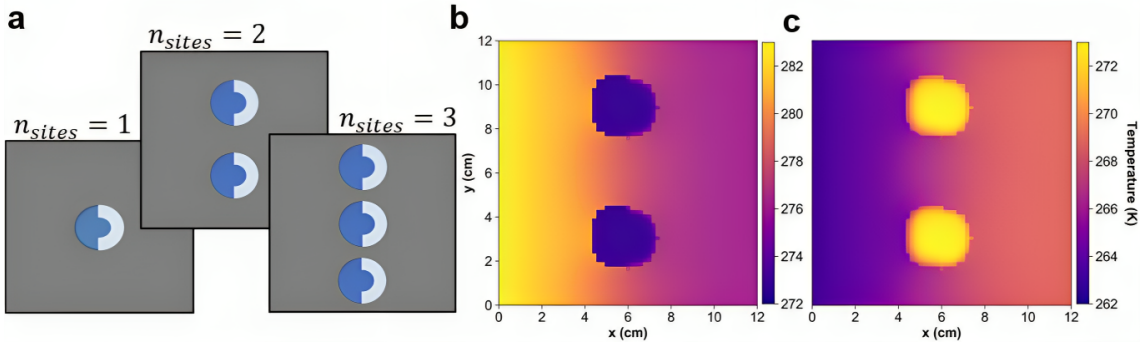


FIGURE 4.5: **(a)** Schematic representation of how the number and shape of the PCM reservoirs were modified. Heat maps for the **(b)** *forward* and **(c)** *reverse* obtained at the instant $t = 60$ s for the case with two PCM regions.

As one may guess, by varying the number of regions covered by PCM and thermal insulator, we are changing the amount of both materials at the same time. This way, we observe a similar behavior in terms of the time it takes to reach the phase transition instant, i.e, a higher number of PCM-covered regions leads to longer periods of time before the phase transition occurs. This way, and taking a look at the rectification curves in figure 4.6(a), it makes sense that increasing the number of PCM regions in the device results in a better rectifying performance (Fig. 4.6(b)).

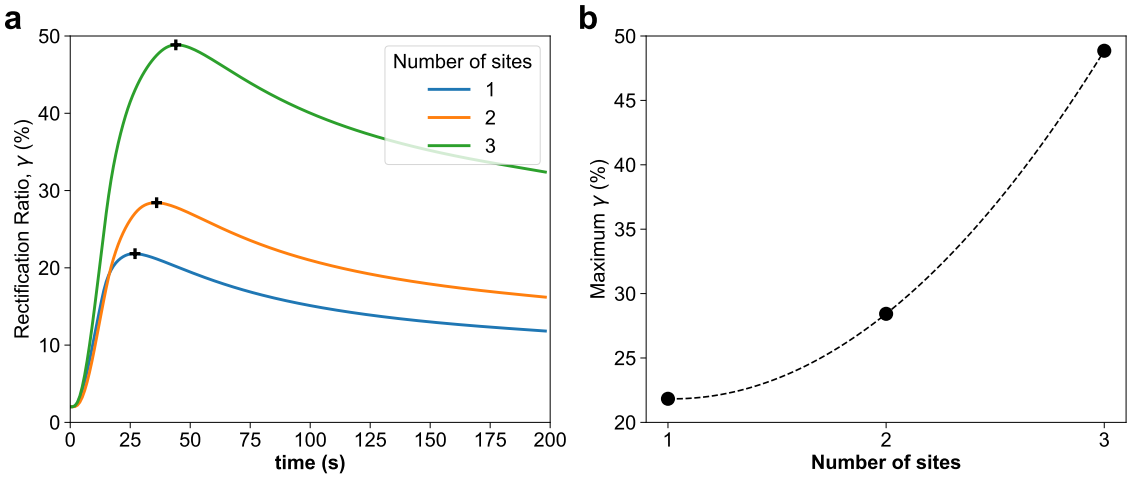


FIGURE 4.6: **(a)** Rectification ratio measured at $L_1$ for different numbers of PCM regions. **(b)** Maximum rectification ratio as a function of the number of sites that contain PCM.

It is important to mention that it was only possible to study the impact of this parameter because the 'unit' of the PCM region had a small enough size that allowed the alignment of multiple regions in the same vertical cross section ($n_{sites} = 3$ case in Fig. 4.5(a)). Naturally, this implies that the maximum amount of total PCM used in these simulations was not as high as in the simulations analyzed in the previous section. As a result, the maximum $\gamma$ obtained was only close to 50%. However, and as clarified before, the goal of these tests was to merely investigate the possibility of using multiple PCM spots with a non-squared shape.

### 4.2.3 Fraction of thermal insulator

Similarly to what was done for the study with the portion of PCM, we also conducted a series of simulations dedicated to evaluate the impact of the amount of thermal insulator for a fixed amount of PCM. For this, a single circularly shaped PCM region surrounded by a 'C-shaped' portion of thermal insulator were used, and the amount of material was varied by changing the thickness of that same region, as schematized in the in inset drawing of Fig. 4.7(a).

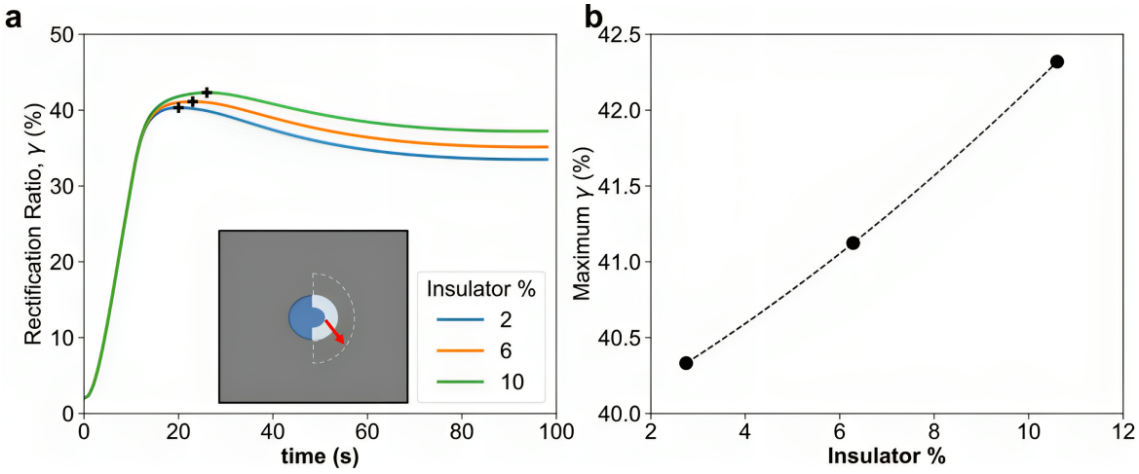


FIGURE 4.7: **(a)** Rectification ratio measured at $L_1$ for different amounts of thermal insulator. **(b)** Maximum rectification ratio as a function of the percentage of thermal insulator amount in the device.

As one can see, the three tested values or thermal insulator amount led to slightly different thermal rectification curves, with the maximum values showing an increasing tendency but only in the 2.5% range (Fig. 4.7(b)). This leads us to the conclusion that the portion of the device that is covered by thermal insulator does not have a very notable effect on the performance of the TD.

## 4.3 Obtaining the transfer function for the final design

Throughout the previous sections multiple adjustments to the initially proposed design were made, with the aim of evaluating the impact of several geometrical parameters in the performance of the device, so that an optimized version could be achieved. Taking all the results into consideration, as well as the many technical complications that could arise if one were to build a physical prototype, we decided to include in the final design three vertically aligned PCM and thermal insulator regions with circular shape (Fig. 4.5(a), $n_{sites} = 3$), where we recall that water and acrylic were the chosen materials for each case, respectively. This choice of design allows us not only to have a decent amount of PCM and thermal insulator spread out across the three regions, but also to facilitate the heat flow in the aluminum block (a design with a single PCM region with oblige to a large size, which would leave small spaces of aluminum on the top and bottom of the structure).

Now that we have a final design and set of materials for the TD, an analysis of its performance for different temperature bias values must be done. In Fig. 4.8(a) we have represented the thermal rectification ratio curves for various values of triggering temperature that were tested, where the intended existence of a maximum value is again visible. Moreover, by plotting the maximum $\gamma$ as a function of $\Delta T$ (Fig. 4.8(b)) we can see the same decreasing tendency observed for the initially proposed design. This shows that the modifications made to set of materials and their geometrical shape did not affect the occurrence of thermal rectification.

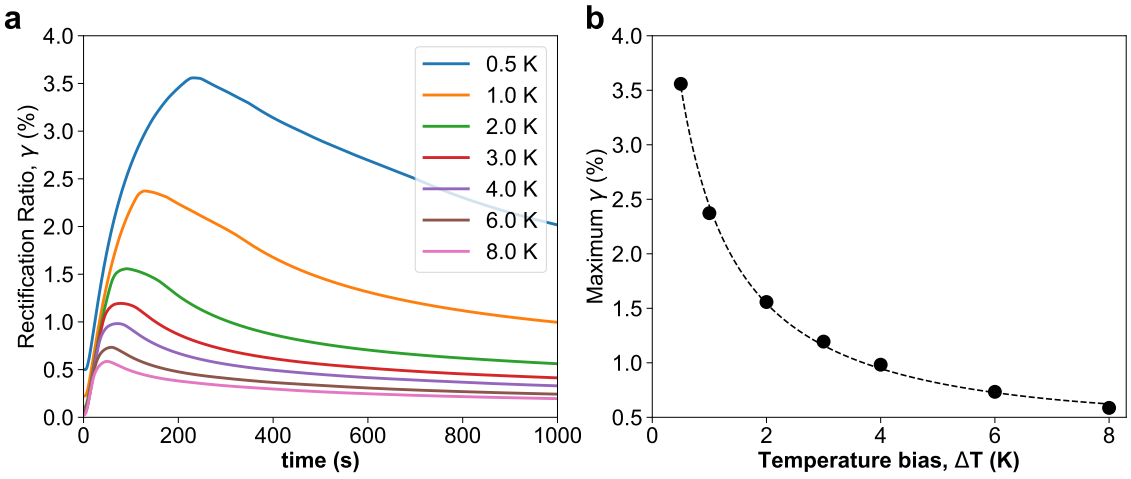


FIGURE 4.8: **(a)** Rectification ratio of the final design measured at $L_1$ for different values of temperature bias. **(b)** Maximum rectification ratio as a function of $\Delta T$.

We now finalize this chapter with the transfer function curve obtained for the final design. As one can see in Fig. 4.9, especially for small temperature bias values, the thermal power density shows a strongly nonlinear response to temperature variation. In fact, the transfer function obtained for the final design is even more nonlinear than the one obtained for the initial design (Fig. 3.8), leading us to conclude that our optimization process was successful.

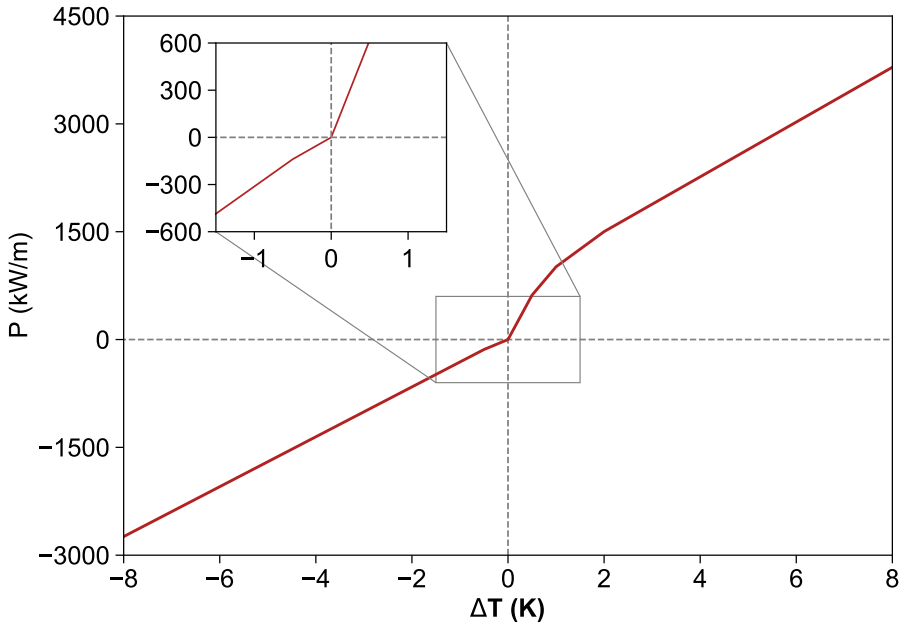


FIGURE 4.9: Transfer function obtained for the final design: temperature dependence thermal power density measured across $L_1$.

# Chapter 5

# From 2D Simulations to 3D Prototyping and Measurement

As the two previous chapters were entirely dedicated to the computational study of a two-dimensional thermal diode structure, we now enter the discussion of the experimental part of this work. The several parameters studied in the numerical simulations, from materials to geometrical aspects, culminated in an optimized design. We mentioned earlier that the decisions made regarding both the thermal insulator to be used and the shape of the PCM-covered regions had in mind the possibility of building a physical prototype of the proposed design. In the following section, we will go through the process of transitioning from the elaborated 2D design to a 3D prototype, the assembly of its several components, and the measurement setup that was conceived for evaluating its performance.

## 5.1 Proposing a design for a 3D prototype

As illustrated in Fig. 5.1, our goal is to find a way of adding a third spatial dimension to the system by introducing a height parameter. However, this modification to the device's structure must be carefully done so that the heat flow rate through the cross section (indicated as $L_1$ in Fig. 5.1), where we intend to measure the thermal power and thermal energy densities, is not compromised by the modified boundary conditions we shall now address.

As we already know from section 3.2, the boundary conditions that allowed us to measure a nonlinear heat flow in the 2D design consist in three (top, bottom and right)

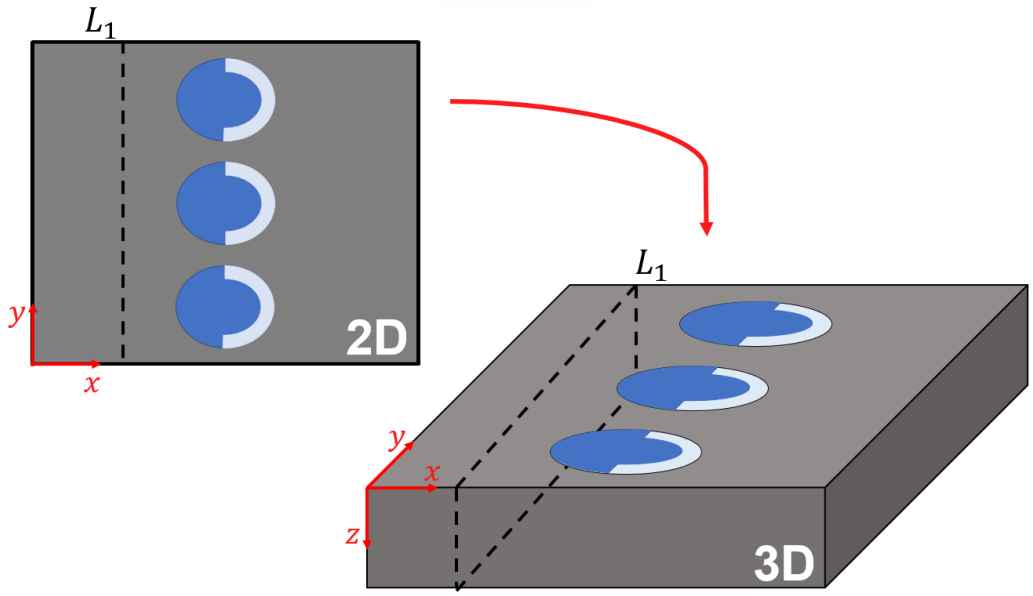


FIGURE 5.1: Schematic representation of the transition from a 2D to a 3D device.

thermally insulated sides, and a fourth side that is subject to a temperature bias whose sign dictates the heat flow direction. Figure 5.2 includes a schematic representation of how one intends to configure the new set of conditions. In the 3D case, we opted for thermally insulating four surfaces (bottom and laterals) of the aluminum block with the aim of providing a more unidirectional heat flow in the $x$ axis direction, similarly to what was done for the 2D device. However, the main condition that had to be implemented due to the transition from a 2D to a 3D prototype has to do with the surface on top of the aluminum block that had to be left open. There were a couple of reasons that supported this configuration, mainly the possibility of maintaining a fixed temperature during the experiments and also the fact that it would facilitate the experimental procedure of assembling the several components and any measuring instruments to be used.

By this point, we also realized that the *forward* and *reverse* configurations would not be possible to be experimentally performed in the same way they were simulated. As in the numerical study, the same surface would be subject to triggering temperature values of different sign, a high complexity setup capable of both cooling and heating a single surface of the device would have to be designed. This way, we opted for designing a structure that included a single heat source, meaning that the '*forward*' and '*reverse*' configurations correspond to heating opposing surfaces of the aluminum component (the heat source in Fig. 5.2 is either placed on the left or right side). However, this drawback forced us to redefine the goal for this part of the project, i.e., since the study of thermal rectification

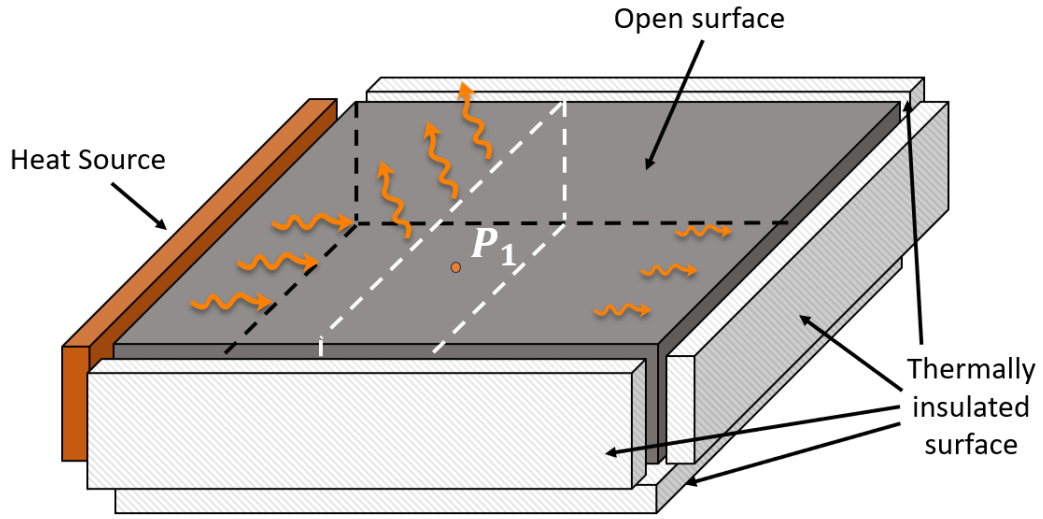


FIGURE 5.2: Schematic representation of the boundary conditions for the 3D case (*forward* configuration).

involves applying both negative and positive temperature biases, and only the second one can be done experimentally, we will only be taking a look at the differences in stored thermal energy when heat flows in opposite directions. Despite this turn of events, one will still be able to determine whether this particular geometry and set of materials, are capable of showcasing nonlinear heat flow.

### 5.1.1 Studying the influence of thickness through 3D COMSOL simulations

As mentioned earlier, before coming up with a definitive design for the three-dimensional version of the device, we must find an accurate value for the new thickness/height parameter that, not only suits an adequate size for a prototype to be tested in the lab (ideally in the same order of magnitude as the width and depth parameters), but also ensures an adequate heat flow rate in the $x$ direction. For this purpose, we performed a simulation in COMSOL *Multiphysics* to evaluate the impact of this new parameter in the heat transfer properties of the system.

COMSOL is a finite element analysis, solver, and simulation software that is widely used for computational studies in physics and engineering applications, especially in the area of thermal management. Unfortunately, simulating heat transfer phenomena and phase transitions in a system that includes both solids (aluminum and acrylic) and liquids (water) is not a trivial task. This way, we ended up simulating a not so complicated scenario: a single aluminum block with the same 12x12 $cm^2$ base used for 2D simulations,

and a variable height, $h$, whose influence on the heat flux we want to evaluate. By running these simulations, we are able to determine the minimum thickness the aluminum block needs to have so that heat escaping through the open surface does not compromise the heat flux in the important direction ($x$), as explained in the previous section. Figure 5.2 provides an illustration for the structure that was simulated, employing the boundary conditions mentioned in the previous section, and indicates the point ($P_1$) where the heat flux was measured. The ambient temperature was set to 0 °C and the left surface is then heated up to 10 °C and heat propagates to the aluminum block through convective heat flux. This simulation ran for a period of 100 s at a time step of 0.05 s and, through the `parametric sweep` function of COMSOL, it was repeated for several values of height, ranging from 0.018 to 0.18 cm. In these simulations we were interested in measuring the total heat flux magnitude (kW/m$^2$) at the central point of the block ($P_1$ in Fig. 5.2), which has a $z$ coordinate that depends on the thickness of the system. The heat flux *vs* time curves obtained for the various values of thickness that were tested are represented in Fig. 5.3(a).

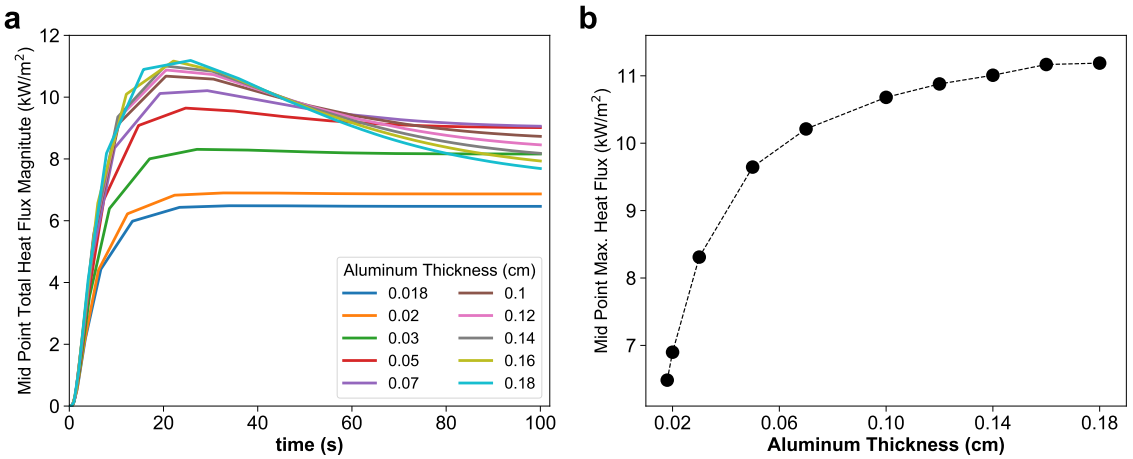


FIGURE 5.3: **(a)** Total heat flux time curves measured at the middle point of the aluminum block for different thickness values. **(b)** Maximum values of total heat flux as a function of the aluminum thickness.

As we can see, an increase in height is translated into different behaviors of the heat flux magnitude curves. We can tell that the smaller values of thickness (0.018-0.03 cm) reach heat flux magnitude values below 8 kW/m$^2$ early on (∼30 s) in the simulation and are held constant until the end. Starting at the case with 0.05 cm of thickness, we begin to obtain a maximum value of heat flux around the t=30 s mark time. For the small values, heat coming from the heat source would escape trough the open top surface without reaching the other side opposite to the one that is being heated, meaning that the heat

flow at the central point is constant. On the other hand, for the higher values of thickness, a maximum heat flux magnitude is measured due to heat that reaches the right boundary and flows back in the opposite direction before being dissipated trough the open boundary. Since we are measuring the total heat flow in all directions, this means that we have heat coming from an additional direction that adds up to the magnitude that was measured for the smaller cases. Plotting the maximum values as a function of thickness, we obtain the curve in Fig. 5.3(b) where we can see that, from a thickness of 0.10 cm, the maximum heat flux magnitude starts to converge to a value close to 11 $kW/m^2$. Nevertheless, the important information that we can extract from these results is the certainty that an aluminum thickness higher than the maximum 0.18 cm that were tested, is enough to have heat flow across the full length of the device, allowing us to perform a reliable study of heat transfer on that same direction.

## 5.2 Final design and finished product

We are now in conditions of presenting a final design (Fig. 5.4) that merges the last geometry studied in the 2D simulations and the necessary conditions for the 3D transition mentioned in the previous section.

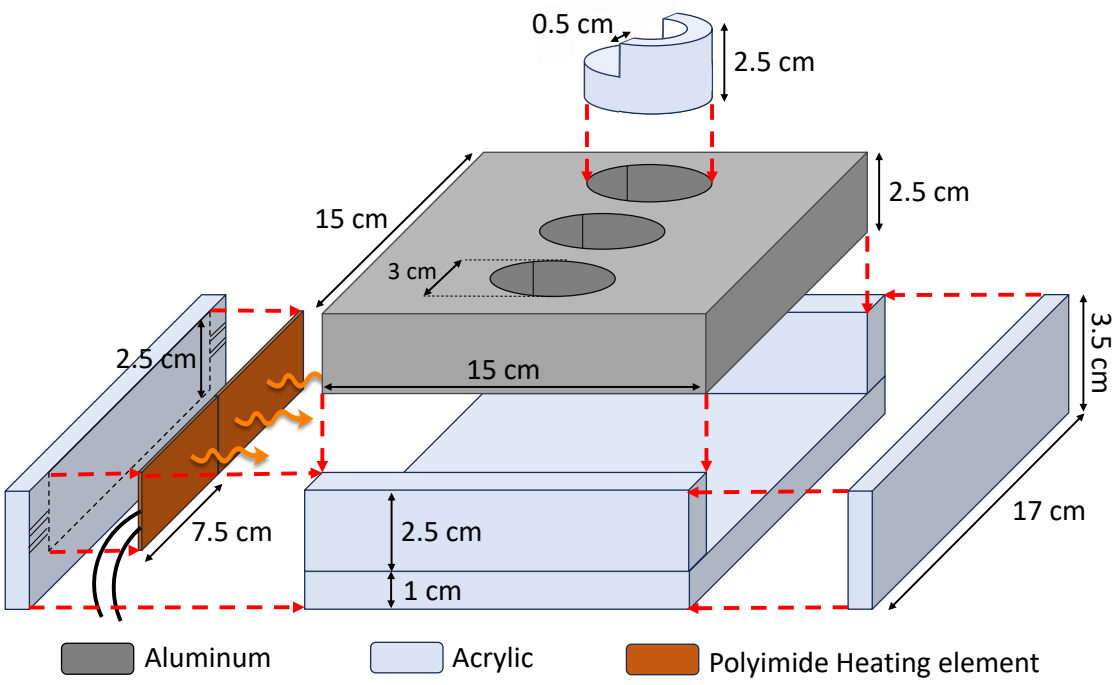


Figure 5.4: Final design of the proposed TD system and schematic representation of how its several components are assembled.

As labeled in Fig. 5.4, the final proposal for the prototype consists in a 15x15x2.5 $cm^3$ aluminum block with three equally spaced circular holes with a 3 cm diameter that provide the space to put in the thermal insulating "cells" made of acrylic, which are then filled with water. From the illustration we can see that these components have the shape of half a cylindrical shell (0.5 cm of thickness), except for the bottom part where a thin acrylic lid was glued to the shell to prevent water leakage. For that same reason, thermal paste is spread on the interface between the aluminum holes and the acrylic shells. The other component of the prototype corresponds to the acrylic box that was built for the boundary condition of thermally insulated bottom and side surfaces to be satisfied. Lastly, two polyimide heating elements are placed in a way that fully covers the surface we want to heat. It is important that the dimensions of the several components do not correspond exactly to the ones that were used for the simulations. This so happens because some of the components, namely the heating elements and the acrylic cylinder, were only available in limited sizes, which meant that a few adjustments to the dimensions of the aluminum block and acrylic box had to be made.

## 5.3 Evaluating the thermal properties of the prototype

In the following section, we go through the acquisition system that allowed us to measure the thermal properties of the presented design and give a detailed description of the various steps of the experimental procedure that were followed in order to obtain those measurements.

### 5.3.1 Acquisition system and experimental procedure

As previously stated, the goal for this part of the project was redefined to determine whether the prototype that was designed showcased differences in thermal energy density depending on the direction of heat flow that was imposed. This study can be achieved by monitoring two important factors:

- the water/ice temperature to verify the occurrence of a phase transition;
- the temperature in certain locations of the aluminum so that we can calculate temperature gradients and work out how the thermal energy density changed over time.

To this end, an appropriate data acquisition setup was developed, as can be seen in Figures 5.5 (scheme) and 5.6 (picture), with every component labeled. Using both the photo of the setup and its schematic representation as a guide, we now describe the experimental procedure for obtaining the referred temperature measurements while simultaneously describing the role of each instrument.

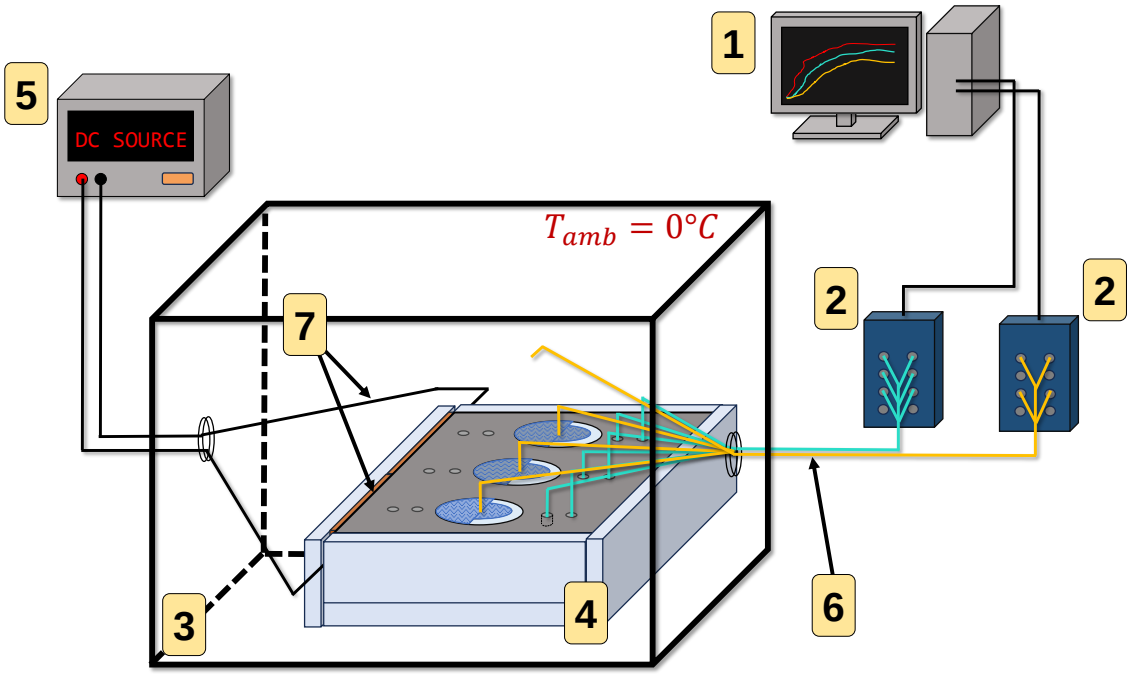


FIGURE 5.5: Schematic representation for the measurement setup. **(1)** Computer with PicoLog 6 for temperature data acquisition; **(2)** Picolog TC-08; **(3)** TMAX temperature test chamber; **(4)** Prototype; **(5)** Tenma: 72-13310 DC Power Supply; **(6)** RS type K thermocouples; **(7)** Polymide heating element.

to facilitate the temperature measurements, a series of holes, visible in Fig. 5.5, with a 0.2 cm diameter and 1 cm of depth that were carved for the thermocouples* (6) to be in direct contact with the aluminum. This also ensures that we are measuring the heat only coming from the aluminum and minimizes the impact of the open surface in the measurements.

Before the prototype (4) is taken to the temperature control chamber (3) and the experience is initiated, the acrylic cells are filled with water, with a thermocouple carefully placed in the middle of each one (as illustrated in Fig. 5.5), and left in a freezer until the water is fully turned into ice. Given the fact that water expands when it turns into ice, a

*A thermocouple is a sensor that, as a result of the Seebeck effect, produces a voltage proportional to the temperature difference between its two metal junctions and that can be used to measure temperature

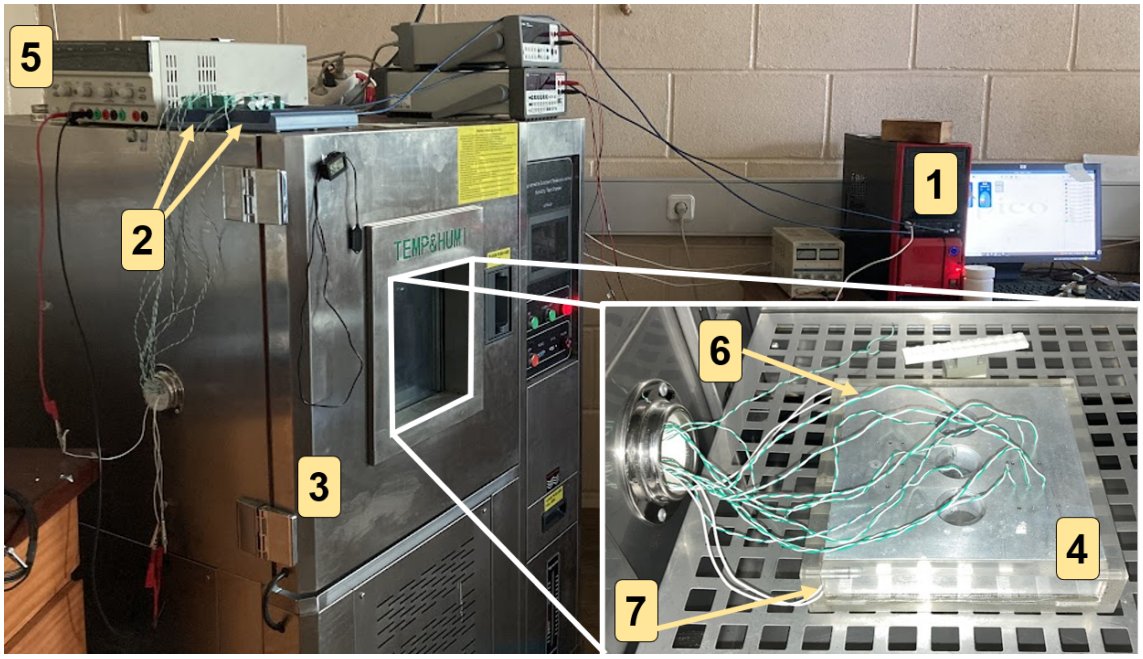


FIGURE 5.6: Measurement setup in the lab. **(1)** Computer with PicoLog 6 for temperature data acquisition; **(2)** Picolog TC-08; **(3)** TMAX temperature test chamber; **(4)** Prototype; **(5)** Tenma: 72-13310 DC Power Supply; **(6)** RS type K thermocouples; **(7)** Polymide heating element.

few tests were made in order to find out the appropriate water volume to be poured into each cell to tackle the risk of overflow and water leakage during the heating process.

The next step is to place the prototype inside the temperature control chamber (3) and assemble the data acquisition setup and heating circuit. Firstly, we begin by inserting the thermocouples (6-green) in the correspondent holes (as we can see in the inset of Fig. 5.6 and connecting them to one of the Picolog TC-08 devices (2). These devices are then connected to a computer with the PicoLog 6 (1) program installed, which displays the temperature values of the several thermocouple channels as a function of time. The thermocouples that come together with the prototype from the freezer (6-yellow) are also connected to the TC-08 device, and their temperature measurements are displayed in the same plot. Depending on the heat flow direction mode, *forward* or *reverse*, the thermocouples are arranged differently (Fig. 5.7) and the reason for this will be discussed in Section 5.4. Lastly, the polyimide heating elements are connected in series and powered by a DC power supply at 24 V.

Once all the components are assembled and every connection is established, the temperature control chamber (3) is turned on and a fixed temperature test, set for 0 °C, is initiated. Since the chamber is initially at ambient temperature and the components that came out of the freezer had temperatures below -5 °C, the heating circuit (5 + 7) was turned

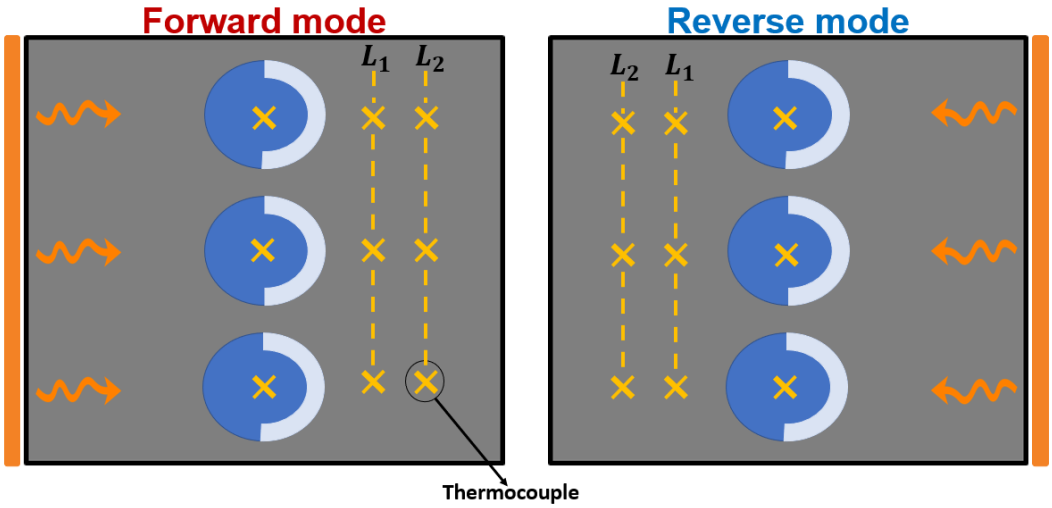


FIGURE 5.7: Schematic representation of the experimental differences between the *forward* and *reverse* configurations and how the thermocouples are placed in both cases.

on only when the temperature of all the components was stabilized. For this purpose, an additional thermocouple was placed freely inside the chamber to control its temperature with the same PicoLog program (1). Once this condition was met, the heating circuit was manually turned on, and this instant marked the beginning of the experiment. Once the heat flow starts, the experiment is only concluded once the temperature of all the components stabilizes again, but at a higher value. All of these steps correspond to a single test of a heat direction mode, i.e., every time one wants to test either the *forward* or *reverse* configuration, the whole process has to be repeated, and the only difference is the orientation of the aluminum block, which is equivalent to changing the heaters from one surface to the opposite one (Fig. 5.7).

### 5.3.2 Data analysis

The resulting data from the acquisition system is saved on a .csv file containing eleven columns: one for time (s) and ten for the temperature measurements from each thermocouple. To analyze this data, we developed a Python sctipt using the *Pandas*, *NumPy* and *Matplotlib* frameworks responsible for: importing the .csv files and converting them into data frames; filtering the data only measured after the heat elements were turned on; separating the temperature data relative to the water cells from the aluminum temperature data; and making temperature *vs time* plots, such as the one in Fig. 5.8. A Python Jupyter Notebook was then used for calculating and plotting the thermal power and thermal energy densities.

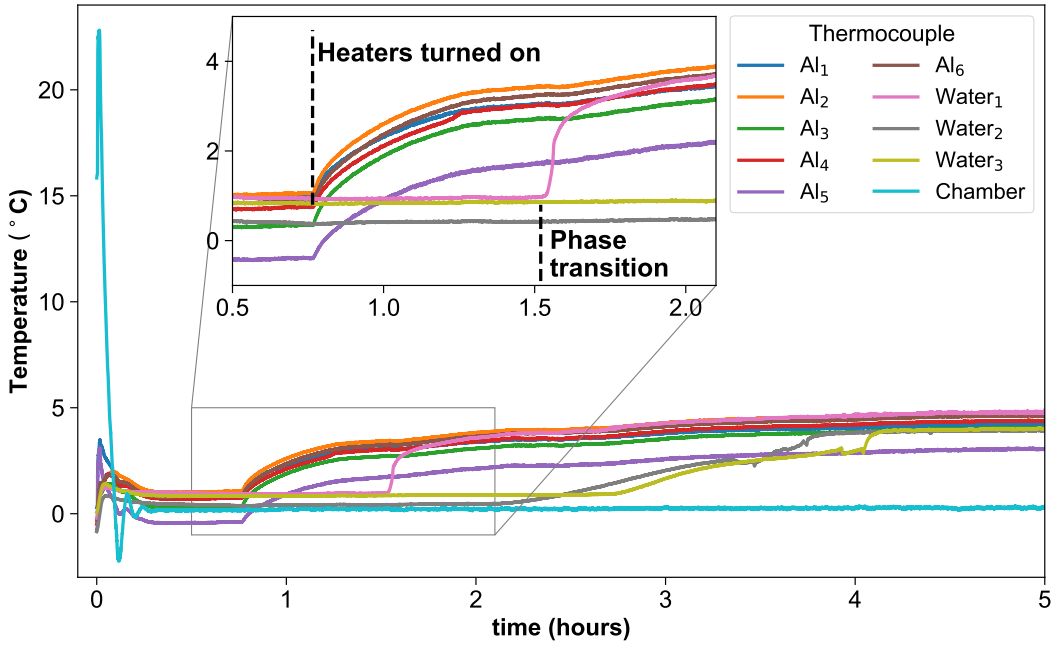


FIGURE 5.8: Example of the temperature plots obtained with the data gathered from the Picolog6 program after one trial of the experiment.

## 5.4 Results and discussion

As mentioned in section 5.3.1, we performed temperature measurements in specific regions of the prototype in order to study its thermal properties. Figure 5.7 illustrates the different thermocouple arrangements along two critical lines where we want to evaluate the differences in thermal power and thermal energy densities.

Firstly, using the temperature data that was collect from the three thermocouples along the $L_1$ and $L_2$ cross sections, for both the *forward* and *reverse* configurations, the average temperature for each case was calculated, and the obtained results are shown as temperature variation curves in Fig. 5.9(a). This plot shows that the boundary conditions that were discussed in the previous section allowed the intended heat flow across the device and led to a temperature variation of 3 °C. Additionally, one can see notable differences not only between the two heat propagation modes, but also between the two lines where the temperature was measured, which provides an early indication of an asymmetrical heat transfer process.

Moreover, one can also see in Fig. 5.9(a) the representation of the temperature variation measured in the central acrylic cell containing ice/water. Since the ambient temperature and heating elements have the same conditions for both heat direction modes, the

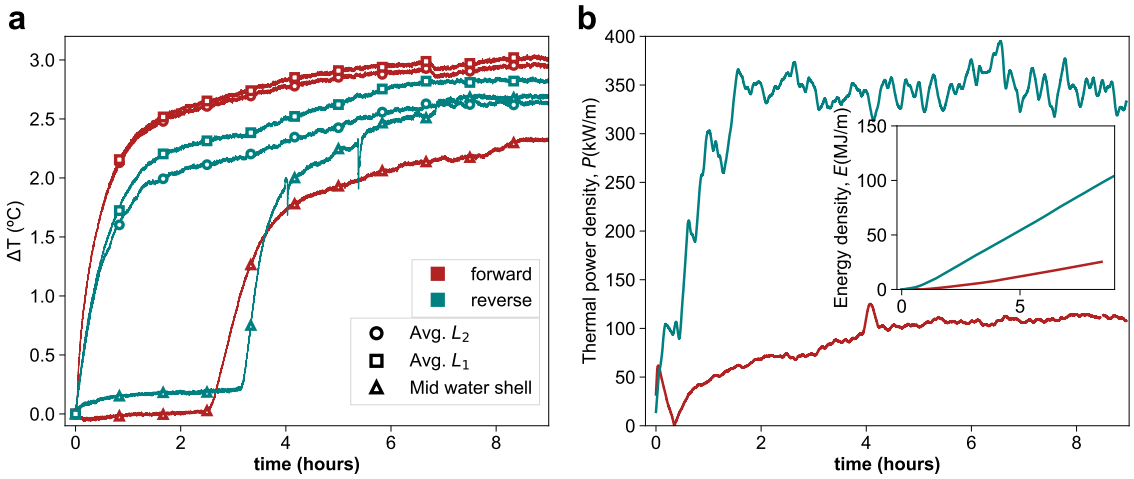


FIGURE 5.9: **(a)** Average temperature measurements from the three thermocouples placed along $L_1$ and $L_2$, and in the central PCM cell.**(b)** Thermal power density computed for the region between $L_1$ and $L_2$ the correspondent thermal energy density (inset).

fact that one can identify a slight difference regarding the phase transition instant, also indicates the statement that the device has a preferential heat flux direction.

However, the confirmation that we were able to conceive a prototype with nonlinear heat transfer properties is given by the thermal power density and thermal energy density, similarly to was done for the 2D simulations. This way, we computed these quantities for the region formed by the $L_1$ and $L_2$ lines of thermocouples (Fig. 5.7), which has a thickness of 1.0 cm. The obtained results are displayed in Fig. 5.9. Regarding the thermal power density, which measures the heat flow rate across this area per unit length, we can see that a difference of 200 kW/m is kept between the two modes for the majority of the experiment duration. Then, using eq. 3.2 the thermal power energy was calculated and, as shown in the inset of Fig. 5.9(b), we were able to measure much higher values of stored thermal energy for the *reverse* mode, surpassing the 100 MJ/m. Having such differences between the two modes of heat propagation, one can conclude that the goal of building a device that showcased a preferential direction to heat flow was fulfilled.

# Chapter 6

# Conclusions and Future Work

As we navigate the demands of contemporary high-performance devices, the need for advanced thermal management systems remains crystal clear. In this context, the use of PCM-based thermal diodes has emerged as a promising solution since they can effectively utilize the distinct heat-absorption and heat-release properties of PCMs during phase transitions. In a world where compact electronic devices dominate, PCM-based TDs have shown promising results in the maintenance of optimal operating temperatures and the enhancement of energy efficiency. This way, we conducted a series of simulations and experiments that allowed us to go from the study of a two-dimensional TD to the design, build, and measurement of a 3D prototype.

In this thesis, we began by presenting the concept of a 2D PCM-based thermal rectifier. This design consisted of a squared sink made of a thermal conductive material, with equally spread PCM reservoirs placed along the middle cross section that are surrounded by a thermal insulating material. This structure was designed to conceive spacial asymmetry in thermal conductivity, fulfilling the main criterion to achieve thermal rectification. The first set of simulations was run for a geometry where the set of materials was aluminum, acrylic, and water, corresponding to the thermal conductor, thermal insulator, and PCM, respectively. Testing it for a temperature bias of $\Delta T = \pm 10$ K, we obtained a massive difference in thermal energy density between the *forward* and *reverse* heat direction configurations. Then, representing the rectification ratio as a function of the temperature bias, we discovered that a higher rectifying performance is associated with higher triggering temperatures, and 60% maximum value was reached for a $\Delta$T=0.5 K. The plot of the transfer function confirmed that the tested design had the desired nonlinear profile

characteristic of thermal rectifiers. Regarding the impact of geometrical parameters and properties of the device on its performance, the main outcomes of this study were:

- using a thermal insulator other than vacuum has no significant impact on the difference between the thermal energy densities of the *forward* and *reverse* configurations. This way, acrylic came as a natural choice since it is easy to machine, cheap, and hydrophobic.
- the increase of the percentage of the device's area that is occupied by PCM leads to an increase in both the time period that precedes the phase transition (0-8 hours) and the thermal rectification ratio (12-170%);
- increasing the fraction of thermal insulator also results in a performance increase, however not as significant as the fraction of PCM (40-42.5%).

Taking into account all these results and envisioning the construction of a physical prototype, we ended up using circular-shaped PCM reservoirs with surrounding acrylic shells. Having this final design and verify its nonlinear transfer function, a series of COMSOL simulations were conducted with the goal of finding the minimum thickness that a three-dimensional version of the device needed to have. After making some adjustments to the design to account for technical issues, the device was built, and the assembled measurement setup allowed us to measure the temperature variations and compute thermal and power densities for the two directions of heat flow. It was found that the ice-water phase transition, paired with the asymmetric design of the thermal insulator shells, led to differences in thermal power and thermal energy densities between the two configurations (200 kW/m), showcasing the desired nonlinear thermal properties of the device.

As for **future work**, one must mention steps that are important to fulfill not only to better explain the results obtained throughout this project but also to broaden its set of conclusions and make it a more relevant study. Firstly, and regarding the computational work that was presented, a more in-depth study of the influence of geometrical parameters, namely varying the shape of the PCM and insulator cells, on rectification performance would be a fine addition to this work. Testing the final geometry for other phase change materials whose solid-liquid phase transition occurs at different critical temperatures would also help to understand the range of temperatures in which the device can operate. As to the practical-related work, the one job that would certainly help in the optimization of the device design is the COMSOL simulation that supported the transition

from a 2D to a 3D geometry. Since we only simulated a quite simplified version of the prototype, figuring out a way of simulating the heat transfer phenomena, maybe using a different software, of the complete structure would be ideal. Now, in terms of the practical work, building a measurement and acquisition setup capable of imposing a negative temperature bias would be the ideal way of implementing thermal diode conditions and testing the rectification performance of our device.

# Appendix A

# Modelling of 2D thermal systems

In this Appendix we briefly described the Python framework *heatrapy* that was implemented to build a computational model able to simulate thermal transfer processes in a 2D thermal diode structure.

## A.1 *Heatrapy*, a Python framework

*Hetrapy* stands for HEAt TRAnsfer in PYthon. It is a framework that simulates 1D and 2D heat transfer processes using the finite difference method. *Heatrapy* includes both the modeling of caloric effects and incorporation of phase transitions [75].

The building block of an *heatrapy* module is a thermal object. For each thermal object, one defines a range of discrete space, where each point incorporates thermal properties, power sources and temperature. Boundary conditions can be defined and also changed at any time. There are several methods available in this framework that can change the state of each point, materials properties, and power sources. In the case of phase transitions, *heatrapy* incorporates them according to the latent heat data of used materials, which can be accessed through an external database. This framework includes two different types of thermal object classes: `SingleObject` and `SystemObjects`, available for both 1D and 2D systems. In this work the class `SingleObject2D` was used. Essentially, this class returns the temperature as a function of time for each space point in the material by numerically solving the two-dimensional heat conduction equation, which is given by

$$\rho C_p \frac{\partial T}{\partial t} - k \left( \frac{\partial^2 T}{\partial x^2} + \frac{\partial^2 T}{\partial y^2} \right) - \dot{Q} = 0, \tag{A.1}$$

where $\rho$ is the density of the material, $C_p$ is the specific heat, $T$ is the temperature, $k$ is the thermal conductivity *, and $\dot{Q}$ is a temperature-dependent heat source, $\dot{Q} = \dot{Q}_0 + q(T - T_{amb})$.

The `SingleObject2D` class can be initialized according to the following code block:

```
object = SingleObject2D(
    amb_temperature,        # ambient temperature of the whole system
    material='Cu',          # background material
    dx=0.01,                # space step along the x-axis
    dy=0.01,                # space step along the y-axis
    dt=0.1,                 # time step
    size=(10, 10),          # lengths in x and y directions (spacial steps)
    file_name=None,         # name of the .csv file to store data
    boundaries=(0, 0, 0, 0),# temperature boundary conditions (left, right,
    bottom top)
    Q=[],                   # fixed heat source coefficient
    Q0=[],                  # temperature dependent heat source coefficient
    initial_state=False,    # initial state of materials
    materials_path=False,   # materials database path
    draw=['temperature', 'materials'], # list of online plots
    draw_scale=None
)
```

After the initialization we end up with only a 2D block of a chosen material. To build a system composed of different materials with different shapes one can perform changes in selected pieces of the background material, and this can be done by applying the `change_material` function to the previously defined function

```
object.change_material(
    shape = 'square',       # or 'circle' is the shape of the new material
    material = 'Cu',        # material
    initial_point = (x,y),  # initial point where the shape is being drawn
    length = (dx,dy),       # length of the square sides
    state = False
)
```

*Given the thermal conductivity vector $\vec{k} = (k_x, k_y)$, and considering an isotropic heat flow, one can consider $k_x = k_y = \equiv k$.

Now, after the structure to be studied is complete one can compute the heat transfer phenomena using the `compute` method:

```
object.compute(
    time_interval = 30000,
    write_interval = 100,
    solver = 'explicit_k(x)',       # 'explicit_general' is the default
    verbose = False
)
'''
It computes the system for *time_interval* and writes to *file_name* every *
    write_interval* time steps.
'''
```

In all the simulations, `'explicit_k(x)'` was the used solver. This is a Crank-Nicolson finite finite difference method and is appropriate for systems with spacial-dependent thermal conductivity.

As an example, the code below computes 100 seconds of a copper 2D solid with a water circle and an Aluminum square. The structure and output at the end of the computation are shown in fig. A.1.

```
>>> import heatrapy as htp
>>> example = htp.SingleObject2D(
...     293,
...     material='Cu',
...     boundaries=(300, 0, 0, 0),
...     size=(20, 20)
... )
>>> example.change_material(
...     material='Al',
...     shape='square',
...     initial_point=(5, 2),
...     length=(4, 4)
... )
>>> example.change_material(
...     material='water',
...     shape='circle',
```

```
...     initial_point=(5, 13),
...     length=4
... )
>>> example.compute(100, 10)
```

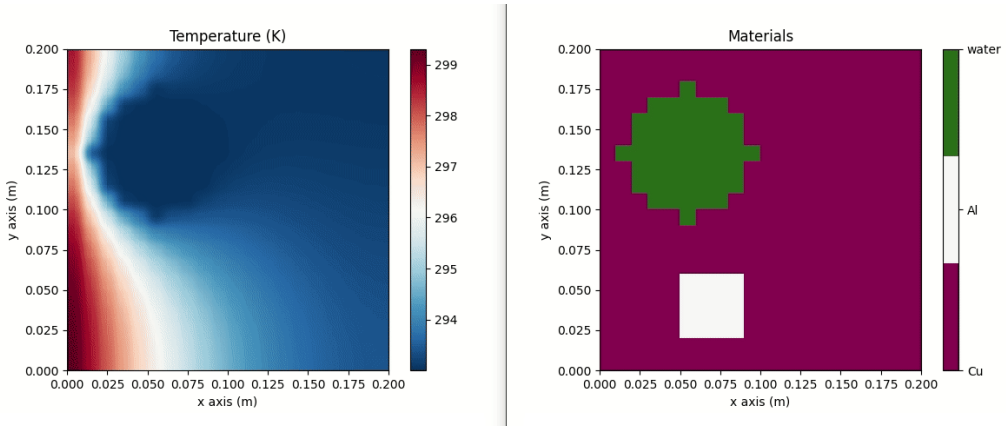


FIGURE A.1: Output example of a *heatrapy* simulation.

If one wishes to study the time evolution of the temperature in certain sites of the system, a filename must be provided in the initialization step and then the temperature data for each point is written to '.csv' file at the provided writing interval.

# Appendix B

# Simulation code

In this appendix, some portions of the code used to simulate a thermal diode, using the Python framework *heatrapy* are presented. In section B.1, the code used to validate the initially proposed TD structure is shown. In section B.2, an example of a script to study a certain geometrical parameter is presented. For every script, the output is a '.csv' file with the temperature values for each point of 61x61 mesh over time.

## B.1 Validation code

```
import heatrapy as htp
import os

file_name = os.path.basename(__file__)
mode = file_name.split('_')[-1]
mode = mode.split('.')[0] # sets the forward or reverse mode
database_pcm = 'database_pcm/' # imports the materials database

def create_Al_base(mode):
    '''
    Create base structure of the heatrapy object
    Set boundary conditions depending on the diode mode
    Set time step
    '''
    if mode=='forward':
        t_boundary = 283
```

```
    else:
        t_boundary = 263
    system = htp.SingleObject2D(
        272.9,
        material='Al',
        dx=0.002,dy=0.002,
        dt=0.01,
        size=(61, 61),
        file_name="Data_files/validation_{}.csv".format(mode),
        boundaries=(t_boundary, 0, 0, 0),
        Q=[],Q0=[],
        initial_state=False,
        materials_path=database_pcm,
        draw=[]
    )

    return system

def create_PCM_spots(system):
    '''
    Creates the three squares with PCM material
    '''
    system.change_material(shape='square', material='water', initial_point=(23,6)
    , length=(12,9), state=False)
    system.change_material(shape='square', material='water', initial_point
    =(23,26), length=(12,9), state=False)
    system.change_material(shape='square', material='water', initial_point
    =(23,46), length=(12,9), state=False)

def create_insulating_capsules(system):
    '''
    Creates the three parts of thermal insulator that surround the PCM spot
    '''
    system.change_material(shape='square', material='vacuum', initial_point
    =(23,3), length=(15,3), state=False)
    system.change_material(shape='square', material='vacuum', initial_point
    =(23,15), length=(15,3), state=False)
```

```
49      system.change_material(shape='square', material='vacuum', initial_point
        =(35,3), length=(3,15), state=False)
        system.change_material(shape='square', material='vacuum', initial_point
        =(23,35), length=(15,3), state=False)
51      system.change_material(shape='square', material='vacuum', initial_point
        =(23,23), length=(15,3), state=False)
        system.change_material(shape='square', material='vacuum', initial_point
        =(35,23), length=(3,15), state=False)
53      system.change_material(shape='square', material='vacuum', initial_point
        =(23,43), length=(15,3), state=False)
        system.change_material(shape='square', material='vacuum', initial_point
        =(23,55), length=(15,3), state=False)
55      system.change_material(shape='square', material='vacuum', initial_point
        =(35,43), length=(3,15), state=False)

57  def compute_heat_transfer(system,total_time,dt):
        '''
59      Computes heat transfer of the system by solving the 2D heat equation using an
         explicit finite element method
        '''
61      system.compute(total_time, dt, solver="explicit_k(x)")

63  def main():
        system1 = create_Al_base(mode)
65      system2 = create_PCM_spots(system1)
        system3 = create_insulating_capsules(system2)
67      compute_heat_transfer(system3,30000, 100)
    main()
```

## B.2 Parameter variation code

In this section we only include the code used to study one of the parameters mentioned in section 4.2, which is the percentage (or area) of PCM content. The first block of code is the script for one value, and the second block was used to run several scripts in parallel, where each one corresponds to a different value of the tested parameter. The other simulations can be performed by making slight changes to these files.

```
    import heatrapy as htp
import matplotlib.pyplot as plt
import os

cwd = os.getcwd()
database_pcm = f'{cwd}/database_pcm/'
mode = file_name.split('_')[-1]
mode = mode.split('.')[0] # sets the forward or reverse mode

if mode=='forward':
        t_boundary = 283
    else:
        t_boundary = 263

system = htp.SingleObject2D(
    272.9,
    material='Al',
    dx=0.002,dy=0.002,
    dt=0.01,
    size=(61, 61),
    file_name="Data_files/Acrylic_side15_{}.csv".format(mode),
    boundaries=(t_boundary, 0, 0, 0),
    Q=[],Q0=[],
    initial_state=False,
    materials_path=database_pcm,
    draw=['materials']
    )

system.change_material(shape='square', material='Acrylic', initial_point=(23,35),
     length=(15,3), state=False)
system.change_material(shape='square', material='Acrylic', initial_point=(23,23),
     length=(15,3), state=False)
system.change_material(shape='square', material='Acrylic', initial_point=(35,23),
     length=(3,15), state=False)
system.change_material(shape='square', material='water', initial_point=(23,26),
    length=(12,9), state=False)

system.compute(30000, 100, solver="explicit_k(x)")
```

```
import multiprocessing
import os

# Creating a dictionary with the format {mode:side}
bias = ['forward','reverse']
side = [15,19,23,27,31,35,39] # length of the PCM square side

all_processes = []
for b in bias:
    for s in side:
    all_processes.append('simulations/simulation_Acrylic_{}_side{}.py'.format(b,s
    ))

all_processes = tuple(all_processes)

# This block of code enables us to call the script from command line.

def execute(process):
    os.system(f'python3 {process}')

process_pool = multiprocessing.Pool(processes = 14)
process_pool.map(execute, all_processes)
```

# Bibliography


[1] J. Lin, X. Liu, S. Li, C. Zhang, and S. Yang, "A review on recent progress, challenges and perspective of battery thermal management system," *International Journal of Heat and Mass Transfer*, vol. 167, 3 2021. [Cited on page 1.]

[2] K. Zhang, Y. Zhang, J. Liu, and X. Niu, "Recent advancements on thermal management and evaluation for data centers," *Applied Thermal Engineering*, vol. 142, pp. 215–231, 9 2018.

[3] R. Wrobel, "A technology overview of thermal management of integrated motor drives – electrical machines," *Thermal Science and Engineering Progress*, vol. 29, 3 2022. [Cited on page 1.]

[4] E. Walsh and R. Grimes, "Low profile fan and heat sink thermal management solution for portable applications," *International Journal of Thermal Sciences*, vol. 46, pp. 1182–1190, 11 2007. [Cited on page 1.]

[5] C. Nadjahi, H. Louahlia, and S. Lemasson, "A review of thermal management and innovative cooling strategies for data center," *Sustainable Computing: Informatics and Systems*, vol. 19, pp. 14–28, 9 2018. [Cited on page 1.]

[6] S. V. Garimella, T. Persoons, J. A. Weibel, and V. Gektin, "Electronics thermal management in information and communications technologies: Challenges and future directions," *IEEE Transactions on Components, Packaging and Manufacturing Technology*, vol. 7, pp. 1191–1205, 8 2017. [Cited on page 1.]

[7] I. Sauciuc, R. Prasher, J.-Y. Chang, H. Erturk, G. Chrysler, C.-P. Chiu, and R. Mahajan, "Thermal performance and key challenges for future cpu cooling technologies," *Proceedings of the ASME Summer Heat Transfer Conference*, vol. 2, pp. 353–364, 01 2005. [Cited on page 1.]

[8] M. Y. Wong, C. Y. Tso, T. C. Ho, and H. H. Lee, "A review of state of the art thermal diodes and their potential applications," *International Journal of Heat and Mass Transfer*, vol. 164, 1 2021. [Cited on pages xiii, 2, 8, 9, 12, 13, 14, and 15.]

[9] N. A. Roberts and D. G. Walker, "A review of thermal rectification observations and models in solid materials," *International Journal of Thermal Sciences*, vol. 50, pp. 648–662, 2011. [Cited on page 2.]

[10] M. Peyrard, "The design of a thermal rectifier," *Europhysics Letters*, vol. 76, pp. 49–55, 10 2006. [Cited on pages 2 and 8.]

[11] C. Dames, "Solid-state thermal rectification with existing bulk materials," *Journal of Heat Transfer*, vol. 131, pp. 1–7, 6 2009. [Cited on pages 2, 20, and 24.]

[12] D. Sawaki, W. Kobayashi, Y. Moritomo, and I. Terasaki, "Thermal rectification in bulk materials with asymmetric shape," *Applied Physics Letters*, vol. 98, 2 2011. [Cited on page 2.]

[13] W. Kobayashi, D. Sawaki, T. Omura, T. Katsufuji, Y. Moritomo, and I. Terasaki, "Thermal rectification in the vicinity of a structural phase transition," *Applied Physics Express*, vol. 5, 2 2012.

[14] R. Chen, Y. Cui, H. Tian, R. Yao, Z. Liu, Y. Shu, C. Li, Y. Yang, T. Ren, G. Zhang, and R. Zou, "Controllable thermal rectification realized in binary phase change composites," *Scientific Reports*, vol. 5, 3 2015. [Cited on pages xiv, 2, 21, and 37.]

[15] G. Wehmeyer, T. Yabuki, C. Monachon, J. Wu, and C. Dames, "Thermal diodes, regulators, and switches: Physical mechanisms and potential applications," *Applied Physics Reviews*, vol. 4, no. 4, p. 041304, 11 2017. [Online]. Available: https://doi.org/10.1063/1.5001072 [Cited on pages xiii, 5, 6, 7, and 8.]

[16] K. Klinar and A. Kitanovski, "Thermal control elements for caloric energy conversion," *Renewable and Sustainable Energy Reviews*, vol. 118, 2 2020. [Cited on page 6.]

[17] S. Lee, K. Hippalgaonkar, F. Yang, J. Hong, C. Ko, J. Suh, K. Liu, K. Wang, J. J. Urban, X. Zhang, C. Dames, S. A. Hartnoll, O. Delaire, and J. Wu, "Anomalously low electronic thermal conductivity in metallic vanadium dioxide," *Science*, vol. 355, no. 6323, pp. 371–374, 2017. [Online]. Available: https://www.science.org/doi/abs/10.1126/science.aag0410 [Cited on pages xiii and 6.]

[18] P. Scherz and S. Monk, *Practical electronics for inventors*. McGraw-Hill Education, 2013. [Cited on pages xiii and 6.]

[19] T. Swoboda, K. Klinar, A. S. Yalamarthy, A. Kitanovski, and M. M. Rojo, "Solid-state thermal control devices," *Advanced Electronic Materials*, vol. 7, 3 2021. [Cited on pages 7 and 8.]

[20] J. Kimling, R. B. Wilson, K. Rott, J. Kimling, G. Reiss, and D. G. Cahill, "Spin-dependent thermal transport perpendicular to the planes of co/cu multilayers," *Physical Review B - Condensed Matter and Materials Physics*, vol. 91, 4 2015. [Cited on pages xiii and 7.]

[21] J. Shin, J. Sung, M. Kang, X. Xie, B. Lee, K. M. Lee, T. J. White, C. Leal, N. R. Sottos, P. V. Braun, and D. G. Cahill, "Light-triggered thermal conductivity switching in azobenzene polymers," *Proceedings of the National Academy of Sciences*, vol. 116, no. 13, pp. 5973–5978, 2019. [Online]. Available: https://www.pnas.org/doi/abs/10.1073/pnas.1817082116 [Cited on pages xiii and 7.]

[22] M. A. Beasley, S. L. Firebaugh, R. L. Edwards, A. C. Keeney, and R. Osiander, "Mems thermal switch for spacecraft thermal control," *MEMS/MOEMS Components and Their Applications*, vol. 5344, p. 98, 1 2004. [Cited on page 7.]

[23] J. Bartlett, G. Hardy, I. Hepburn, R. Ray, and S. Weatherstone, "Thermal characterisation of a tungsten magnetoresistive heat switch," *Cryogenics*, vol. 50, pp. 647–652, 9 2010. [Cited on page 7.]

[24] L. Zurdo, L. Chej, A. Monastra, and F. Carusela, "Thermal diode assisted by geometry under cycling temperature," 2023. [Cited on pages xiii and 10.]

[25] H. Kang and F. Yang, "Thermal rectification via heterojunctions of solid-state phase-change materials," *Physical Review Applied*, vol. 10, 8 2018. [Cited on pages xiii and 10.]

[26] J.-J. Greffet, "Electrons and phonons," *Microscale and Nanoscale Heat Transfer*, pp. 37–54, 2007. [Cited on page 10.]

[27] J. D. Renteria, D. L. Nika, and A. A. Balandin, "Graphene thermal properties: Applications in thermal management and energy storage," pp. 525–547, 12 2014. [Cited on page 11.]

[28] X. K. Chen, Z. X. Xie, Y. Zhang, Y. X. Deng, T. H. Zou, J. Liu, and K. Q. Chen, "Highly efficient thermal rectification in carbon/boron nitride heteronanotubes," *Carbon*, vol. 148, pp. 532–539, 7 2019. [Cited on pages xiii and 11.]

[29] H. Wang, S. Hu, K. Takahashi, X. Zhang, H. Takamatsu, and J. Chen, "Experimental study of thermal rectification in suspended monolayer graphene," *Nature Communications*, vol. 8, 6 2017. [Cited on pages xiii and 11.]

[30] F. Giazotto and F. S. Bergeret, "Thermal rectification of electrons in hybrid normal metal-superconductor nanojunctions," *Applied Physics Letters*, vol. 103, 12 2013. [Cited on pages xiii and 11.]

[31] S. Li, Z. X. Guo, and J. W. Ding, "Interface thermal transport of graphene-based intralayer heterostructures," *Physica B: Condensed Matter*, vol. 561, pp. 164–169, 5 2019. [Cited on page 11.]

[32] F. Yousefi, M. Shavikloo, and M. Mohammadi, "Non-equilibrium molecular dynamics study on radial thermal conductivity and thermal rectification of graphene," *Molecular Simulation*, vol. 45, pp. 646–651, 5 2019. [Cited on page 11.]

[33] A. Pugsley, A. Zacharopoulos, J. D. Mondol, and M. Smyth, "Theoretical and experimental analysis of a horizontal planar liquid-vapour thermal diode (plvtd)," *International Journal of Heat and Mass Transfer*, vol. 144, 12 2019. [Cited on pages xiii, 11, and 12.]

[34] M. Y. Wong, B. Traipattanakul, C. Y. Tso, C. Y. Chao, and H. Qiu, "Experimental and theoretical study of a water-vapor chamber thermal diode," *International Journal of Heat and Mass Transfer*, vol. 138, pp. 173–183, 8 2019. [Cited on page 11.]

[35] J. B. Boreyko and C. H. Chen, "Vapor chambers with jumping-drop liquid return from superhydrophobic condensers," *International Journal of Heat and Mass Transfer*, vol. 61, pp. 409–418, 2013. [Cited on page 11.]

[36] A. Fiorino, D. Thompson, L. Zhu, R. Mittapally, S. A. Biehs, O. Bezencenet, N. El-Bondry, S. Bansropun, P. Ben-Abdallah, E. Meyhofer, and P. Reddy, "A thermal diode based on nanoscale thermal radiation," *ACS Nano*, vol. 12, pp. 5174–5179, 6 2018. [Cited on pages xiii, 11, and 13.]

[37] G. Xu, J. Sun, H. Mao, and T. Pan, "Highly efficient near-field thermal rectification between insb and graphene-coated sio2," *Journal of Quantitative Spectroscopy and Radiative Transfer*, vol. 220, pp. 140–147, 11 2018. [Cited on page 11.]

[38] E. Nefzaoui, K. Joulain, J. Drevillon, and Y. Ezzahri, "Radiative thermal rectification using superconducting materials," 12 2013. [Online]. Available: http://arxiv.org/abs/1312.3758http://dx.doi.org/10.1063/1.4868251 [Cited on pages 11 and 13.]

[39] Y. A. Çengel and A. J. Ghajar, *Heat and Mass Transfer: Fundamentals and Applications*. McGraw-Hill Education, 2020. [Cited on page 12.]

[40] L. Hu, A. Narayanaswamy, X. Chen, and G. Chen, "Near-field thermal radiation between two closely spaced glass plates exceeding planck's blackbody radiation law," *Applied Physics Letters*, vol. 92, 2008. [Cited on page 12.]

[41] P. van Zwol, K. Joulain, P. Ben-Abdallah, and J. Chevrier, "Phonon-polaritons enhance near field thermal transfer across the phase transition of vo2," vol. 84, 1998. [Online]. Available: https://hal-iogs.archives-ouvertes.fr/hal-00649190 [Cited on page 13.]

[42] P. Ben-Abdallah and S. A. Biehs, "Phase-change radiative thermal diode," *Applied Physics Letters*, vol. 103, 11 2013. [Cited on page 13.]

[43] A. Ghanekar, Y. Tian, M. Ricci, S. Zhang, O. Gregory, and Y. Zheng, "Near-field thermal rectification devices using phase change periodic nanostructure," *Optics express*, vol. 26, no. 2, pp. A209–A218, 2018.

[44] A. Ghanekar, J. Ji, and Y. Zheng, "High-rectification near-field thermal diode using phase change periodic nanostructure," *Applied Physics Letters*, vol. 109, no. 12, 2016.

[45] S. Jia, Y. Fu, Y. Su, and Y. Ma, "Far-field radiative thermal rectifier based on nanostructures with vanadium dioxide," *Optics letters*, vol. 43, no. 22, pp. 5619–5622, 2018. [Cited on page 13.]

[46] S. Basu and M. Francoeur, "Near-field radiative transfer based thermal rectification using doped silicon," *Applied Physics Letters*, vol. 98, no. 11, 2011. [Cited on page 13.]

[47] L. Wang and Z. Zhang, "Thermal rectification enabled by near-field radiative heat transfer between intrinsic silicon and a dissimilar material," *Nanoscale and microscale thermophysical engineering*, vol. 17, no. 4, pp. 337–348, 2013.

[48] G. Xu, J. Sun, H. Mao, and T. Pan, "Highly efficient near-field thermal rectification between insb and graphene-coated sio2," *Journal of Quantitative Spectroscopy and Radiative Transfer*, vol. 220, pp. 140–147, 2018. [Cited on page 13.]

[49] D. Ginsberg, *Physical Properties of High Temperature Superconductors III*, ser. Physical properties of high temperature superconductors. World Scientific, 1992. [Online]. Available: https://books.google.pt/books?id=oLANz-zSdgkC [Cited on page 13.]

[50] J. Khan and M. H. Arsalan, "Solar power technologies for sustainable electricity generation - a review," pp. 414–425, 3 2016. [Cited on page 14.]

[51] T. M. Mahlia, T. J. Saktisahdan, A. Jannifar, M. H. Hasan, and H. S. Matseelar, "A review of available methods and development on energy storage; technology update," *Renewable and Sustainable Energy Reviews*, vol. 33, pp. 532–545, 2014. [Cited on page 14.]

[52] M. Westwood, "Thermal rectification to increase power and efficiency of solar-thermal electricity generation." [Cited on pages xiii and 14.]

[53] B. Zhao, "Thermal diode bridge applied to solar energy harvesting," 2015. [Cited on page 14.]

[54] J. Miller, W. Jang, and C. Dames, "Thermal rectification by ballistic phonons in asymmetric nanostructures," 2009. [Cited on pages xiii and 14.]

[55] I. I. E. Agency, "The future of cooling opportunities for energy-efficient air conditioning together secure sustainable," 2018. [Online]. Available: www.iea.org/t&c/ [Cited on page 15.]

[56] J. S. Brown and P. A. Domanski, "Review of alternative cooling technologies," *Applied Thermal Engineering*, vol. 64, pp. 252–262, 3 2014. [Cited on page 15.]

[57] S. Crossley, N. D. Mathur, and X. Moya, "New developments in caloric materials for cooling applications," *AIP Advances*, vol. 5, 6 2015. [Cited on page 15.]

[58] A. Kitanovski, U. Plaznik, U. Tomc, and A. Poredoš, "Present and future caloric refrigeration and heat-pump technologies," pp. 288–298, 10 2015. [Cited on pages xiii and 15.]

[59] W. de Vries and T. H. van der Meer, "Application of peltier thermal diodes in a magnetocaloric heat pump," *Applied Thermal Engineering*, vol. 111, pp. 377–386, 1 2017. [Cited on page 16.]

[60] U. Tomc, J. Tušek, A. Kitanovski, and A. Poredoš, "A new magnetocaloric refrigeration principle with solid-state thermoelectric thermal diodes," *Applied Thermal Engineering*, vol. 58, pp. 1–10, 2013. [Cited on page 16.]

[61] K. Pielichowska and K. Pielichowski, "Phase change materials for thermal energy storage," *Progress in Materials Science*, vol. 65, pp. 67–123, 2014. [Cited on pages 16 and 19.]

[62] D. Fernandes, F. Pitié, G. Cáceres, and J. Baeyens, "Thermal energy storage:"how previous findings determine current research priorities"," *Energy*, vol. 39, no. 1, pp. 246–257, 2012. [Cited on page 16.]

[63] G. A. Lane, *Solar Heat Storage: Volume I: Latent Heat Material*. CRC press, 2018. [Cited on page 17.]

[64] M. F. Demirbas, "Thermal energy storage and phase change materials: An overview," *Energy Sources, Part B: Economics, Planning and Policy*, vol. 1, pp. 85–95, 1 2006. [Cited on page 17.]

[65] F. Agyenim, N. Hewitt, P. Eames, and M. Smyth, "A review of materials, heat transfer and phase change problem formulation for latent heat thermal energy storage systems (lhtess)," *Renewable and sustainable energy reviews*, vol. 14, no. 2, pp. 615–628, 2010. [Cited on page 17.]

[66] A. Sharma, V. V. Tyagi, C. R. Chen, and D. Buddhi, "Review on thermal energy storage with phase change materials and applications," *Renewable and Sustainable energy reviews*, vol. 13, no. 2, pp. 318–345, 2009. [Cited on pages 17 and 18.]

[67] A. M. Khudhair and M. M. Farid, "A review on energy conservation in building applications with thermal storage by latent heat using phase change materials," *Energy conversion and management*, vol. 45, no. 2, pp. 263–275, 2004.

[68] V. V. Tyagi and D. Buddhi, "Pcm thermal storage in buildings: A state of art," *Renewable and sustainable energy reviews*, vol. 11, no. 6, pp. 1146–1166, 2007. [Cited on pages 17 and 18.]

[69] M. Liu, W. Saman, and F. Bruno, "Review on storage materials and thermal performance enhancement techniques for high temperature phase change thermal storage systems," *Renewable and Sustainable Energy Reviews*, vol. 16, pp. 2118–2132, 2012. [Cited on page 18.]

[70] N. Radouane, "A comprehensive review of composite phase change materials (cpcms) for thermal management applications, including manufacturing processes, performance, and applications," *Energies*, vol. 15, 11 2022. [Cited on pages xiii and 19.]

[71] A. Abhat, "Low temperature latent heat thermal energy storage: heat storage materials," *Solar energy*, vol. 30, no. 4, pp. 313–332, 1983. [Cited on page 18.]

[72] Y. Zhang, G. Zhou, K. Lin, Q. Zhang, and H. Di, "Application of latent heat thermal energy storage in buildings: State-of-the-art and outlook," *Building and environment*, vol. 42, no. 6, pp. 2197–2209, 2007. [Cited on page 19.]

[73] L. Shilei, Z. Neng, and F. Guohui, "Impact of phase change wall room on indoor thermal environment in winter," *Energy and buildings*, vol. 38, no. 1, pp. 18–24, 2006. [Cited on pages xiv, 19, and 20.]

[74] R. Kandasamy, X. Q. Wang, and A. S. Mujumdar, "Transient cooling of electronics using phase change material (pcm)-based heat sinks," *Applied Thermal Engineering*, vol. 28, pp. 1047–1057, 6 2008. [Cited on pages xiv and 20.]

[75] D. J. Silva, J. S. Amaral, and V. S. Amaral, "Heatrapy: A flexible python framework for computing dynamic heat transfer processes involving caloric effects in 1.5d systems," *SoftwareX*, vol. 7, pp. 373–382, 1 2018. [Cited on pages 26 and 59.]